

Late-time Spectroscopy of Type Iax Supernovae

Ryan J. Foley^{1,2*}, Saurabh W. Jha³, Yen-Chen Pan¹, WeiKang Zheng⁴,
Lars Bildsten⁵, Alexei V. Filippenko⁴, Daniel Kasen^{6,7,8}

¹*Astronomy Department, University of Illinois at Urbana-Champaign, 1002 W. Green Street, Urbana, IL 61801, USA*

²*Department of Physics, University of Illinois at Urbana-Champaign, 1110 W. Green Street, Urbana, IL 61801, USA*

³*Department of Physics and Astronomy, Rutgers, The State University of New Jersey, 136 Frelinghuysen Road, Piscataway, NJ 08854, USA*

⁴*Department of Astronomy, University of California, Berkeley, CA 94720-3411, USA*

⁵*Kavli Institute for Theoretical Physics and Department of Physics Kohn Hall, University of California, Santa Barbara, CA 93106, USA*

⁶*Department of Physics, University of California, Berkeley, CA 94720, USA*

⁷*Department of Astronomy and Theoretical Astrophysics Center, University of California, Berkeley, CA 94720, USA*

⁸*Nuclear Science Division, Lawrence Berkeley National Laboratory, Berkeley, CA 94720, USA*

Accepted . Received ; in original form

ABSTRACT

We examine the late-time ($t \gtrsim 200$ days after peak brightness) spectra of Type Iax supernovae (SNe Iax), a low-luminosity, low-energy class of thermonuclear stellar explosions observationally similar to, but distinct from, Type Ia supernovae. We present new spectra of SN 2014dt, resulting in the most complete published late-time spectral sequence of a SN Iax. At late times, SNe Iax have generally similar spectra, all with a similar continuum shape and strong forbidden-line emission. However, there is also significant diversity where some SN Iax spectra display narrow P-Cygni features from permitted lines and a continuum indicative of a photosphere at late times in addition to strong narrow forbidden lines, while others have no obvious P-Cygni features, strong broad forbidden lines, and weak narrow forbidden lines. Finally, some SNe Iax have spectra intermediate to these two varieties with weak P-Cygni features and broad/narrow forbidden lines of similar strength. We find that SNe Iax with strong broad forbidden lines also tend to be more luminous and have higher-velocity ejecta at peak brightness. We find no evidence for dust formation in the SN ejecta or the presence of circumstellar dust, including for the infrared-bright SN 2014dt. Late-time SN Iax spectra have strong [Ni II] emission, which must come from stable Ni, requiring electron captures that can only occur at the high densities of a (nearly) Chandrasekhar-mass WD. Therefore, such a star is the likely progenitor of SNe Iax. We estimate blackbody and kinematic radii of the late-time photosphere, finding the latter an order of magnitude larger than the former for at least one SN Iax. We propose a two-component model that solves this discrepancy and explains the diversity of the late-time spectra of SNe Iax. In this model, the broad forbidden lines originate from the SN ejecta, similar to the spectra of all other types of SNe, while the photosphere, P-Cygni lines, and narrow forbidden lines originate from a wind launched from the remnant of the progenitor white dwarf and is driven by the radioactive decay of newly synthesised material left in the remnant. The relative strength of the two components accounts for the diversity of late-time SN Iax spectra. This model also solves the puzzle of a long-lived photosphere and slow late-time decline of SNe Iax.

Key words: supernovae—general, supernovae—individual (PTF09ego, PTF09eyi, PTF10bvr, SN 2002cx, SN 2004cs, SN 2005P, SN 2005hk, SN 2007J, SN 2008A, SN 2008ge, SN 2008ha, SN 2010ae, SN 2011ay, SN 2011ce, SN 2012Z, SN 2014dt)

1 INTRODUCTION

Type Iax supernovae (SNe Iax) are a newly defined class of stellar death (Foley et al. 2013, hereafter F13). These thermonuclear explosions are observationally similar to, but

* E-mail: rfoley@illinois.edu

distinct from, SNe Ia. The main observational differences between the two classes are related to energetics: SNe Iax have peak luminosities, integrated luminosity, and near-maximum ejecta velocities that are substantially lower than that of SNe Ia (e.g., [Filippenko 2003](#); [Li et al. 2003](#); [Jha et al. 2006](#)), with the most extreme members of the class having peak luminosities and ejecta velocities 1% and 20% those of typical SNe Ia, respectively ([Foley et al. 2009, 2010b](#); [Stritzinger et al. 2014](#)).

While SNe Ia and Iax have somewhat similar spectra near maximum brightness (e.g., [Li et al. 2003](#); [Branch et al. 2004](#); [Chornock et al. 2006](#); [Jha et al. 2006](#); [Phillips et al. 2007](#); [Sahu et al. 2008](#); [Foley et al. 2010b, 2013](#); [Stritzinger et al. 2014, 2015](#)), the late-time ($t \gtrsim 200$ d) spectra of SNe Iax are more distinct from SNe Ia and SNe of all other classes ([Jha et al. 2006](#); [F13](#); [McCully et al. 2014b](#)). Specifically, even a year after explosion, SNe Iax lack the strong forbidden Fe lines at blue optical wavelengths ([Fe II] $\lambda 4200$, [Fe III] $\lambda 4700$, and [Fe II] $\lambda 5270$) and still have a continuum and P-Cygni profiles with very low velocities (~ 500 km s $^{-1}$; [Jha et al. 2006](#), hereafter [J06](#)).

The large differences at late times likely point to different explosion mechanisms and progenitors for SNe Ia and Iax. Since the probable progenitor system of one SN Iax (SN 2012Z) has been detected in pre-explosion images ([McCully et al. 2014a](#)), while no progenitor system has yet been detected for SNe Ia even in deep pre-explosion images (e.g., [Li et al. 2011](#); [Kelly et al. 2014](#)), there is additional evidence that SNe Ia and Iax have different progenitor systems, although this difference may be primarily constrained to the companion stars.

Currently, the leading progenitor model for SNe Iax is a C/O white dwarf (WD) accreting material from a He-star donor ([Foley et al. 2009, 2013](#); [Liu et al. 2015](#), although see [Kromer et al. 2015](#)). This model is consistent with all current observational data ([F13](#)) including the probable progenitor detection of SN 2012Z ([McCully et al. 2014a](#), and the non-detection of the progenitor system for SN 2014dt; [Foley et al. 2015](#)).

Because of the low ejecta masses required for some SNe Iax (perhaps as low as $0.1 M_{\odot}$; e.g., [Foley et al. 2009, 2010b](#); [McCully et al. 2014b](#); [Valenti et al. 2009](#)), there is indirect evidence that the progenitor star is not completely disrupted. Models of a C/O WD undergoing a deflagration that does not fully disrupt the progenitor WD (e.g., [Jordan et al. 2012](#); [Kromer et al. 2013, 2015](#)) can explain most of the observations including the low luminosity, low ejecta velocities, and slow late-time luminosity decline. However, additional constraints on the explosion mechanism are required for further progress. The potential detection of the remnant WD years after SN 2008ha exploded ([Foley et al. 2014](#)) would be the most direct indication that some SNe Iax do not completely disrupt their progenitor stars.

Here, we examine the late-time spectra of a sample of 10 SNe Iax to further understand the physical mechanisms of this class of SNe. The diverse spectra at $t > 200$ d after peak brightness provide multiple clues about the explosion and the final fate of the progenitor star.

We describe our sample and data, which includes new observations of SN 2014dt, in Section 2. Section 3 presents various physical quantities for the late-time spectra of SNe Iax and the measurements are analysed in Section 4.

Table 1. SN Iax Maximum-light Parameters

| SN | $M_{V,\text{peak}}$ (mag) | $\Delta m_{15}(V)$ (mag) | v_{ph} (km s $^{-1}$) |
|--------|---------------------------|--------------------------|---------------------------------|
| 2002cx | −17.52 (0.18) | 0.84 (0.09) | −5550 (20) |
| 2005P | ... | ... | ... |
| 2005hk | −18.07 (0.25) | 0.92 (0.01) | −4490 (430) |
| 2008A | −18.16 (0.15) | 0.82 (0.06) | −6350 (160) |
| 2008ge | −17.60 (0.25) | 0.34 (0.24) | ... |
| 2010ae | −15.33 (0.54) | 1.15 (0.04) | −4390 (60) |
| 2011ay | −18.40 (0.16) | 0.75 (0.12) | −5560 (80) |
| 2011ce | ... | ... | ... |
| 2012Z | −18.50 (0.09) | 0.89 (0.01) | −6030 (180) |
| 2014dt | −17.40 (0.50) | ... | ... |

Note. — Uncertainties listed in parentheses.

We discuss our findings in Section 5 and conclude in Section 6.

2 SAMPLE

For our sample, we begin with the data presented by [F13](#), which represents the largest sample of SNe Iax to date. This sample contains 25 SNe Iax, of which 7 have late-time ($t \gtrsim 200$ d) spectra. In addition to the data presented by [F13](#), [Sahu et al. \(2008\)](#), [Foley et al. \(2010a\)](#), [Stritzinger et al. \(2014\)](#), and [Stritzinger et al. \(2015\)](#) present late-time spectra for SNe 2005hk, 2008ge, 2010ae, and 2012Z, which we include here. In addition, we use the updated light-curve parameters for SNe 2010ae and 2012Z ([Stritzinger et al. 2014, 2015](#), respectively).

We add to this sample SN 2014dt, the closest SN Iax yet discovered ([Foley et al. 2015](#)). Below, we present late-time spectra of SN 2014dt.

We also examined the sample of [White et al. \(2015\)](#), which includes a compilation of six SNe identified as SNe Iax that are not in the [F13](#) sample. In Appendix A, we determine that while four are genuine SNe Iax, two are most likely not SNe Iax. Of the genuine [White et al. \(2015\)](#) SNe Iax, two have spectra at $t > 100$ d. However, none is at $t > 125$ d nor has sufficiently high quality for inclusion in this analysis.

The combined sample has 10 SNe Iax with late-time spectra. We give light-curve parameters and maximum-light photospheric velocity measurements for these objects in Table 1. We present the phases of our primarily examined spectra in Table A3.

2.1 SN 2014dt

The newest addition to our sample is SN 2014dt, which was detected in M61 on 2014 October 29.8 (all dates are UT) at $V = 13.6$ mag by [Nakano & Itagaki \(2014\)](#) and promptly classified as a SN Iax by [Ochner et al. \(2014\)](#) from a spectrum obtained 2014 October 31.2. The SN was past peak at discovery and there are no recent nondetections which constrain the date of explosion.

[Foley et al. \(2015\)](#) present a spectrum from 2014 November 18.6, 19.6 rest-frame days after discovery. Using SNID ([Blondin & Tonry 2007](#)), we determine that SN 2014dt

was at a phase of $+23 \pm 7$ d for that spectrum. The classification spectrum, taken at 1.4 rest-frame days after discovery, yields a phase of $+15 \pm 19$ d. Using both constraints, we estimate that SN 2014dt was discovered $+4 \pm 7$ d after maximum brightness, consistent with the photometry. This puts maximum light for SN 2014dt on 2014 October 25 (± 7 d).

At discovery, SN 2014dt had an absolute magnitude $M_V = -16.9 \pm 0.3$ mag, where we use a distance modulus to M61 of 30.45 ± 0.24 mag¹ (Foley et al. 2015).

Since SN 2014dt was discovered close to peak brightness, the discovery magnitude is a reasonable upper limit on the peak magnitude. For the lower limit, we examine the light curves of other SNe Iax, which have a maximum $\Delta m_{15}(V) = 1$ mag (F13). Since the SN was discovered before $+15$ d, a reasonable lower limit is $M_V = -17.9$ mag. We use these limits to set the range of peak absolute magnitudes, $M_V = -17.4 \pm 0.5$ mag.

We obtained a series of low-resolution spectra of SN 2014dt. Here we focus on the late-time spectra obtained from 2015 April 10 through July 24, corresponding to phases of 172 to 270 d after *B*-band maximum brightness. The remainder of our dataset will be presented by Jha et al. (in prep.). The data were obtained with the Goodman spectrograph (Clemens et al. 2004) on the 4 m SOAR telescope, the Robert Stobie spectrograph (Smith et al. 2006) on the 10 m SALT telescope, the Kast double spectrograph (Miller & Stone 1993) on the Shane 3 m telescope at Lick Observatory, and the Low Resolution Imaging Spectrometer (LRIS; Oke et al. 1995) on the 10 m Keck I telescope.

For most data, standard CCD processing and spectrum extraction were accomplished with IRAF². The SALT spectra were partially reduced with PySALT (Crawford et al. 2010). The data were extracted using the optimal algorithm of Horne (1986). Low-order polynomial fits to calibration-lamp spectra were used to establish the wavelength scale, and small adjustments derived from night-sky lines in the object frames were applied. We employed our own IDL routines to flux calibrate the data and remove telluric lines using the well-exposed continua of spectrophotometric standards (Wade & Horne 1988; Foley et al. 2003). Details of our spectroscopic reduction techniques are described by Silverman et al. (2012).

A log of spectral observations is presented in Table A2, and the spectra are shown in Figure 1.

¹ Fox et al. (2015) use a distance modulus of 31.43 mag, which is inconsistent with the Tully-Fisher distance ($\mu = 30.21 \pm 0.70$ mag; Schoeniger & Sofue 1997), the redshift-derived distance (corrected for Virgo infall; $\mu = 30.59 \pm 0.16$ mag), and an expanding photosphere method distance using the SN II 2008in (Bose & Kumar 2014, $\mu = 30.45 \pm 0.10$ mag or $\mu = 30.81 \pm 0.20$ mag, with the difference resulting from different prescriptions and the former being more consistent with external distances for a large sample). Their assumed distance comes from a separate analysis of SN 2008in (Rodríguez et al. 2014). While that distance may be correct, the authors specifically point out that their analysis yields a significant negative extinction for SN 2008in, the only such outlier of their sample.

² IRAF: the Image Reduction and Analysis Facility is distributed by the National Optical Astronomy Observatory, which is operated by the Association of Universities for Research in Astronomy, Inc. (AURA) under cooperative agreement with the National Science Foundation (NSF).

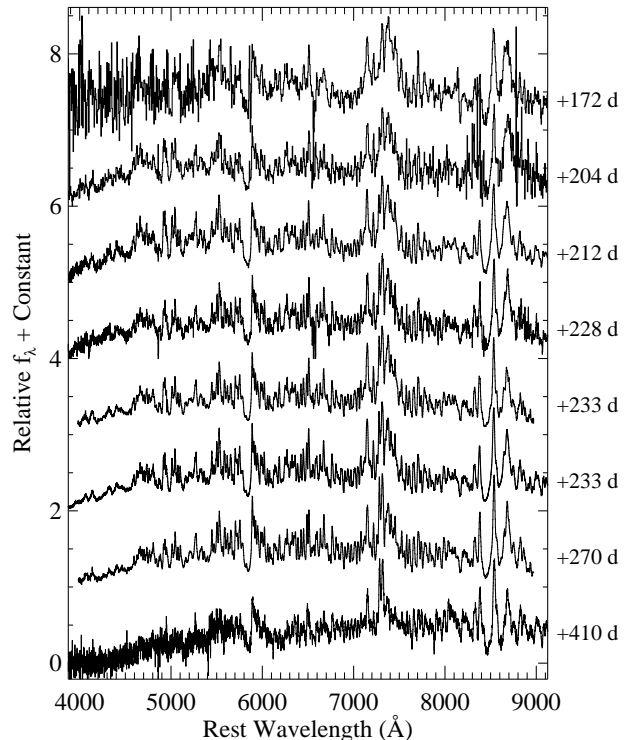


Figure 1. Late-time spectra of SN 2014dt. Each spectrum is labeled by its phase relative to *B*-band maximum brightness. All spectra have a continuum, permitted P-Cygni features, and forbidden lines.

3 PROPERTIES OF LATE-TIME SN Iax SPECTRA

3.1 Spectral Variations Among SNe Iax

The primary difference between maximum-light spectra of different SNe Iax is their ejecta velocity (F13). If a low-velocity SN Iax spectrum is shifted and smoothed to mimic having a higher ejecta velocity, the result will resemble that of a higher-velocity SN Iax spectrum.

At late times, all SN Iax spectra share certain characteristics. There is always a continuum, and the general shapes of the spectra are similar. The spectra all have similar permitted features such as the Ca II near-infrared (NIR) triplet and Na I D. Similarly, every late-time spectrum has at least some indication of [Ca II] emission.

However, the late-time spectra of SNe Iax show significant diversity, and variance beyond that seen near peak brightness. While some late-time spectra have obvious low-velocity (~ 500 km s⁻¹) P-Cygni profiles (e.g., SN 2002cx; J06), others have higher velocities blending these lines (e.g., SN 2008ge; Foley et al. 2010a). In addition to the difference in velocities, there are differences in the strength of forbidden lines. In particular, the [Fe II] $\lambda 7155$, [Ca II] $\lambda\lambda 7291, 7324$, and [Ni II] $\lambda 7378$ features have significantly different line strengths and widths.

Example spectra of objects having (1) high velocity, strong [Ni II], and weak [Ca II] (SN 2008ge), (2) low velocity, weak [Ni II], and strong [Ca II] (SN 2002cx), and (3) intermediate properties (SN 2008A) are displayed in Figure 2.

These three spectra are indicative of the main differences among late-time SN Iax spectra.

SN 2002cx has low velocities at late times resulting in numerous P-Cygni features being visible at all optical wavelengths. It has no obvious [Ni II] $\lambda 7378$ emission, but relatively strong [Fe II] $\lambda 7155$ and [Ca II] $\lambda\lambda 7291, 7324$. SN 2008ge has lines broad enough such that individual P-Cygni profiles are not obvious except for the strongest lines (e.g., Na D and the Ca NIR triplet). None the less, its continuum is consistent with that of SN 2002cx, perhaps indicating that the main difference between SNe 2002cx and 2008ge at late phases is that the latter has higher-velocity material. The [Ni II] $\lambda 7378$ and [Fe II] $\lambda 7155$ features for SN 2008ge are very strong and somewhat strong, respectively, while its [Ca II] $\lambda\lambda 7291, 7324$ emission is barely noticeable as small notches on the wings of the [Ni II] $\lambda 7378$ profile.

SN 2008A is intermediate to SNe 2002cx and 2008ge. It has broad features similar to SN 2008ge, but there are weak, low-velocity P-Cygni profiles superimposed on the broader features. Its [Fe II] $\lambda 7155$ emission is similar to that of both SNe 2002cx and 2008ge, but noticeably narrower than that of SN 2008ge. Its [Ca II] $\lambda\lambda 7291, 7324$ emission is relatively strong. The [Ni II] $\lambda 7378$ emission is sufficiently strong to produce a pronounced “shoulder” on the [Ca II] profile, but is not strong enough to have a defined peak.

Furthermore, there are obvious line shifts between the different spectra. The peaks of the forbidden lines are progressively shifted further to the blue from SN 2008ge to SN 2008A to SN 2002cx.

While there are additional differences between these spectra, as well as for other spectra in our sample, these are the most obvious. They shape the initial investigations discussed below.

3.2 Forbidden-Line Diversity

As noted above, the [Fe II] $\lambda 7155$, [Ca II] $\lambda\lambda 7291, 7324$, and [Ni II] $\lambda 7378$ forbidden lines show significant diversity in the late-time spectra of SNe Iax. Here we fit these features to measure line strengths, velocity shifts, and velocity widths.

We fit multiple Gaussian profiles to all late-time SN Iax spectra in the region 6900 – 7700 Å. Although this ignores other spectral features in this region, the emission in this region is typically well described by emission from only the four features listed above. For some spectra, it was obvious that two components (a “broad” component with a velocity width of ~ 8000 km s $^{-1}$ full width at half-maximum intensity (FWHM), and a “narrow” component with a velocity width of ~ 1000 km s $^{-1}$ FWHM) were necessary, with each narrow/broad feature having the same kinematic properties (velocity shift and velocity width) as the other narrow/broad features. No spectrum has obvious broad [Ca II] emission.

We fit the spectra with 4 kinematic parameters (2 each for the narrow and broad components), 5 parameters to describe the line strengths (fixing each [Ca II] line to have the same flux), and a constant flux offset, for a total of 10 parameters. For a subset, the fitting procedure could not distinguish between a constant flux offset and low-flux, extremely broad, often extremely offset emission features; in such cases (SNe 2002cx, 2010ae, and 2011ce), we fixed these broad features to have zero flux, effectively removing the broad components from the fit. We also tried fitting each feature sepa-

rately, but found the parameters for the features from each kinematic component to be essentially identical. The best-fitting models are shown in Figure 3 and the parameters are listed in Table A3.

In each case, the 10-parameter fit is generally a good description of the data. In some cases (particularly SNe 2002cx, 2005hk, 2010ae, 2011ce, and 2014dt), there are additional features, mostly corresponding to permitted Fe II lines (J06), which are not well fit by this model. We do not attempt to account for these features. In particular, we note that as seen in the spectral sequence of SN 2014dt (Section 3.3; Figure 8), there appears to be a feature at roughly the position of [Ca II] $\lambda 7324$ which is unlikely to be that line. This feature is present in the 172-day spectrum of SN 2014dt, but there is no similar line at 7291 Å. In all later epochs (from +203 d onward), the [Ca II] $\lambda 7291$ line is present and of similar strength to [Ca II] $\lambda 7324$, though we caution that the other, contaminating line may result in suboptimal fitting of these features, but should not significantly affect our results for the spectra we examine. None the less, future investigations may employ a more detailed analysis where other lines, including permitted features, are also fitted.

From the fitting, we can see at least three types of behaviour. There are SNe Iax where the narrow components dominate, corresponding to SNe 2002cx, 2005hk, 2010ae, and 2011ce; SNe Iax where the broad components dominate, corresponding to SNe 2008ge, 2011ay, and 2012Z; and SNe Iax where the narrow and broad components are roughly similar in strength, corresponding to SNe 2005P, 2008A, and 2014dt. These correspond to the rough characterisation made at the beginning of Section 3 and in Figure 2.

While several SNe have no discernible broad components, all SNe have at least some narrow emission. We can remove the need for narrow components in SN 2011ay if we do not require that the broad components have the same velocity shifts and velocity widths. However, the broad components appear to have the same widths and shifts for all other SNe Iax, and all other SNe Iax require at least some narrow emission for a reasonable fit. As such, we include the narrow lines in its fit, but caution overinterpretation of the strength of these features.

Below, we analyze the correlations between these parameters.

3.3 Spectral Evolution with Time

Only a few SNe Iax have multiple late-time spectra. Of these objects, SN 2002cx has two spectra separated by only 50 d (+227 and +277 d; J06). SN 2005hk has at least 4 late-time spectra, spanning a period of +230 d to +455 d (although the last spectrum with a detected continuum is at +403 d; McCully et al. 2014b). SN 2008A has four late-time spectra spanning +200 d to +283 d (McCully et al. 2014b). SN 2012Z has two spectra at +215 and +248 d (a difference of only 33 d; Stritzinger et al. 2015). Finally, SN 2014dt has multiple late-time spectra spanning +172 to +410 d. For SNe 2002cx and 2012Z, the time spans are relatively short, and there is no obvious difference in the spectra at our disposal. Therefore, there are three SNe worth further investigation: SNe 2005hk, 2008A, and 2014dt.

For SN 2005hk, there is very little difference in the spec-

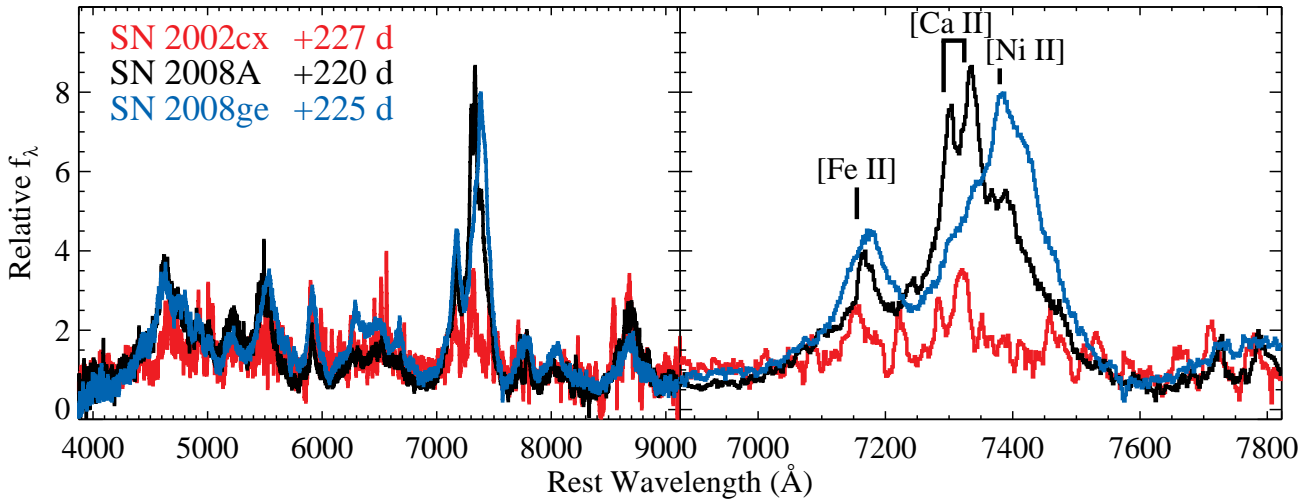


Figure 2. Late-time spectra of SNe 2002cx at a phase of +227 d, (red curve), 2008A at a phase of +220 d (black curve), and 2008ge at a phase of +225 d (blue curve). The left panel shows the entire optical region, while the right panel displays the region containing the [Fe II] λ 7155, [Ca II] $\lambda\lambda$ 7291, 7324, and [Ni II] λ 7378 features (all labeled). The SN 2002cx spectrum has a relatively high signal-to-noise ratio (S/N), and the small-amplitude features in the SN 2002cx spectrum are mostly real (J06). This figure displays the heterogeneous late-time spectra of SNe Iax.

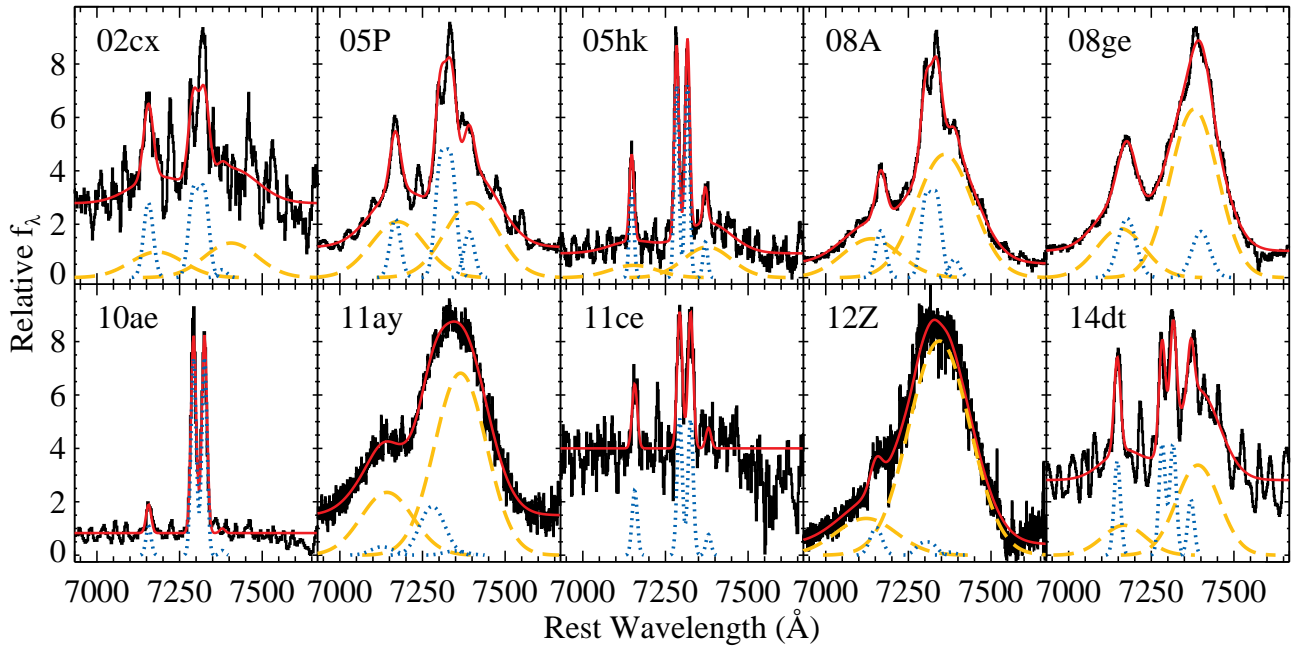


Figure 3. Late-time spectra of SNe Iax (black). Each panel displays the spectrum of a different SN. The red curve corresponds to the best-fitting 10-parameter model of the forbidden lines. The blue dotted curves and the gold dashed curves correspond to the individual narrow and broad components, respectively.

tral appearance between +230 and +403 d (Figure 4). Although roughly 6 months has passed between these epochs, and the SN is nearly twice as old in the second epoch as in the first and has faded significantly, the spectra are nearly identical.

Examining the differences between the two spectra (Figure 4), we note that there is a slight difference in the continuum strength, which may be the result of small errors in flux calibration or a slight change to the tempera-

ture of the photosphere. Additionally, the [Ca II] $\lambda\lambda$ 7291, 7324 lines have a smaller equivalent width (EW) in the later spectrum (Figure 4). This difference is caused by the [Ca II] lines becoming narrower, with the FWHM decreasing from 290 km s^{-1} to 230 km s^{-1} , and moving slightly to the red (as determined by simultaneously fitting both lines with Gaussians), with the velocity shift increasing from -360 km s^{-1} to -180 km s^{-1} (where a negative velocity indicates a blueshifted feature; Figure 5). Similar behaviour

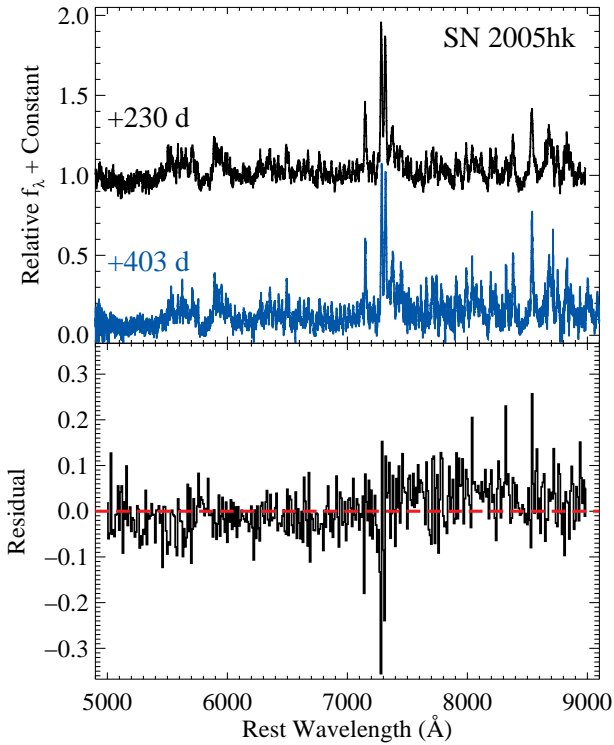


Figure 4. *Top panel:* Late-time spectra of SN 2005hk at phases of roughly +230 (top, black curve) and +403 d (bottom, blue curve), respectively. The spectra are nearly identical in appearance despite the SN fading significantly between these epochs. *Bottom panel:* Residual spectrum for these two spectra where the earlier spectrum is subtracted from the later spectrum. The main difference is in the [Ca II] $\lambda\lambda 7291, 7324$ feature. This difference is the result of the lines becoming somewhat narrower with time (see Figure 5).

is seen in the permitted lines. The decrease in velocity for both the permitted and narrow forbidden lines suggests a physical connection. We note that these velocity shifts are unlikely to be caused by reddening from newly formed dust; in that case, we would expect the lines to shift to the blue (e.g., [Smith et al. 2008](#)).

SN 2008A, unlike SN 2005hk, has significant spectral evolution between +200 and +283 d. Again, SN 2008A has faded significantly between these epochs. While most of the spectrum is nearly identical during this time (Figure 6), the strengths of the forbidden lines ([Fe II] $\lambda 7155$, [Ca II] $\lambda\lambda 7291, 7324$, and [Ni II] $\lambda 7378$) change dramatically between the three epochs (at +200, +224, and +283 d). Most of this evolution occurs between +224 and +283 d, with only minor changes to the features between +200 and +224 d. While the forbidden-line strengths change, the SN does not transition to (or from) a spectrum more similar to SN 2002cx or SN 2008ge; SN 2008A always has relatively strong narrow and forbidden lines.

Examining the forbidden lines in detail (Figure 7), we see that the narrow components (see Section 3.2) of the lines all get stronger (in EW) by factors of ~ 2 –5 between +224 and +283 d. This is most obvious in the [Ca II] doublet, which increases in strength by a factor of ~ 4 and is clearly the dominant feature in the +283 d spectrum. The broad

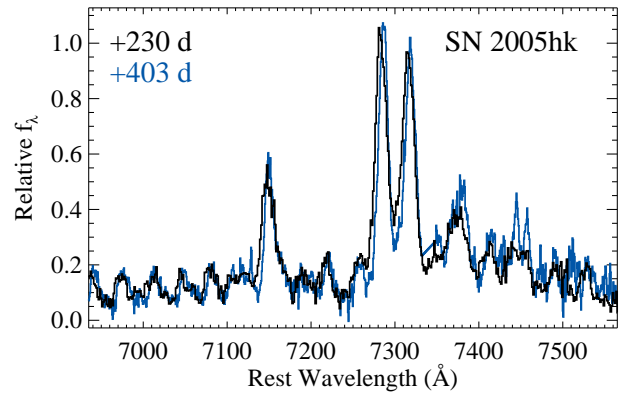


Figure 5. Late-time spectra of SN 2005hk at phases of roughly +230 (black curve) and +403 d (blue curve), respectively. The later spectrum has narrower and more blueshifted features for both the permitted and forbidden lines.

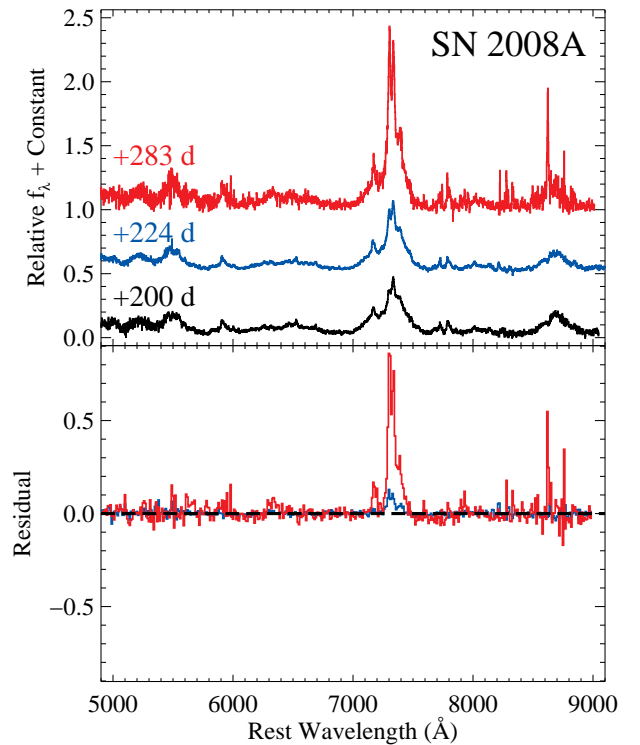


Figure 6. *Top panel:* Late-time spectra of SN 2008A at phases of roughly +200 (bottom, black curve), +224 d (middle, blue curve), and +283 d (top, red curve), respectively. The spectra are nearly identical, except for at wavelengths of 7000 – 7600 Å. *Bottom panel:* Residual spectra for these spectra where the +200 d spectrum is subtracted from the later spectra. The main differences are in [Fe II] $\lambda 7155$, [Ca II] $\lambda\lambda 7291, 7324$, and [Ni II] $\lambda 7378$, with the later spectra having generally stronger lines.

[Fe II] feature is roughly the same strength in both spectra, but the broad [Ni II] feature is $\sim 50\%$ stronger in the later spectrum. This behaviour may be the result of the continuum fading while the narrow features stay relatively constant in flux.

Similar to SN 2005hk, the narrow forbidden lines be-

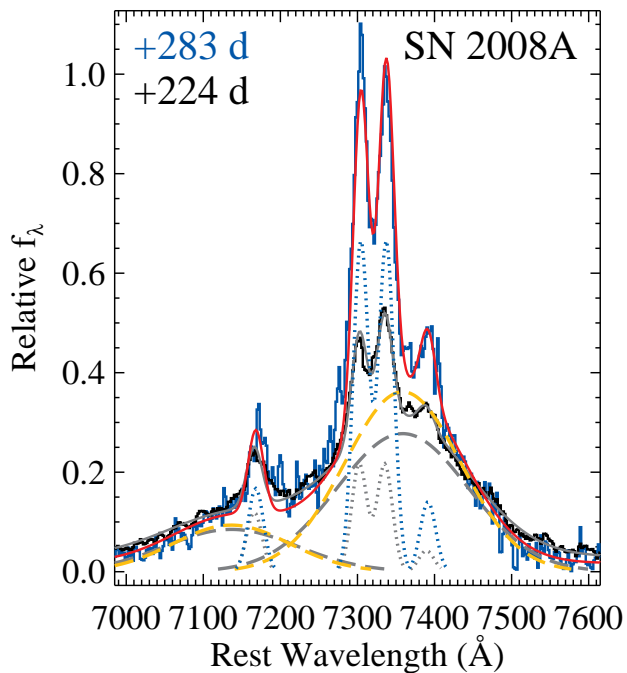


Figure 7. Late-time spectra of SN 2008A at phases of roughly +200 (black curve) and +283 d (dark-blue curve), respectively. Also shown are 10-parameter model spectra (see Section 3.2) in solid grey and red, respectively. The components corresponding to broad [Fe II] $\lambda 7155$ and [Ni II] $\lambda 7378$ are shown with long-dashed lines, with the grey and gold curves corresponding to the +200 and +283 d spectra, respectively. Similarly, the narrow [Ca II] $\lambda\lambda 7291, 7324$ and [Ni II] $\lambda 7378$ are shown as dotted lines, with the light-blue and grey curves corresponding to the +200 +283 d spectra, respectively.

come slightly more redshifted with time (from $+470 \text{ km s}^{-1}$ to $+550 \text{ km s}^{-1}$), but the line widths do not significantly change. The velocity widths of the broad components do not significantly change either. However, detailed modeling of the full complex, including permitted-line emission, may reveal subtle shifts.

Finally, SN 2014dt has the best spectral sequence of any SN Iax at late times. The details of the spectral evolution will be presented by Jha et al. (in prep.); here we focus on the region around the forbidden lines already identified. We display that spectral region in Figure 8. In Figure 8, we also show the residual spectra compared to the +270 d spectrum.

Notably, the spectra do not evolve from being similar to SN 2002cx into being similar to SN 2008ge (or vice versa; see Figure 2). The main changes are the continued decrease in a broad feature that is presumably [Ni II] $\lambda 7378$ with perhaps some contribution from [Fe II] $\lambda 7155$, and the strengthening of narrow [Ca II] $\lambda\lambda 7291, 7324$. Despite these noticeable differences between different phases, there is very little spectral evolution between +203 and +410 d. The 172-day spectrum is less similar to the other spectra and likely is still transitioning into being a true “late-time” spectrum. This relative stability implies that a single spectrum taken after about 200 d relative to maximum brightness is sufficient to characterise the late-time spectrum of a SN Iax. While this statement is consistent with our findings for SNe 2005hk and 2014dt, more data will be necessary to determine if the evo-

lution seen in SN 2008A typically occurs primarily around +270 d or continues steadily between +230 and +270 d.

Despite the evolutionary changes seen in SNe 2005hk, 2008A, and 2014dt, they are all relatively small and any such late-time evolution should not significantly affect our results below.

3.4 Velocity Shifts

As is evident from Figures 2 and 3, as well as Table A3, there are large differences in the forbidden-line shifts in late-time SN Iax spectra. These shifts can be caused by the motion of the progenitor system or asymmetries in the explosion.

In addition to forbidden-line shifts, the permitted features are at different velocities for different SNe. To determine the relative velocity shifts between spectra, we cross-correlated the SN 2005hk spectrum and other spectra. From the measured lag, we can directly measure the velocity shift. SN 2005hk was used since it has (1) a very high-S/N spectrum; (2) relatively low-velocity features, allowing for precise measurements of any shifts; and (3) both narrow and broad forbidden lines.

Performing the cross-correlation, we decided to examine different wavelength ranges. We measured cross correlations using essentially all data (4600 – 9000 Å), a blue region (4600 – 6500 Å, limited on the red side to avoid any possible correlation with galactic H α emission), a red region (7600 – 9000 Å, bounded on the blue side to avoid the strong forbidden lines discussed above), a forbidden-line region (6900 – 7600 Å), as well as disjoint 1000 Å regions starting at 5000 – 6000 Å and ending at 8000 – 9000 Å.

Unsurprisingly, many of the derived cross-correlation velocities are strongly correlated with each other. Interestingly, the forbidden-line region is uncorrelated with all nonoverlapping regions. The highest correlation is with the red region: a correlation coefficient of 0.14. The forbidden-line region has a higher anticorrelation with the 5000 – 6000 Å region (correlation coefficient of -0.51).

However, half of the SN Iax sample (SNe 2002cx, 2005P, 2005hk, 2010ae, 2011ce, and 2014dt) have forbidden-line shifts similar to that of the permitted lines. Notably, these are the SNe Iax with the weakest broad emission lines and their forbidden-line shifts are primarily determined from the narrow forbidden lines. The remaining SNe have forbidden-line shifts that are significantly offset from their permitted-line shifts, as determined by cross correlation.

Examining the velocity shifts for the narrow forbidden lines as determined in Section 3.2, the permitted line shifts are now relatively correlated with a correlation coefficient of 0.47. Comparing these values, the outliers are SNe 2008A, 2008ge, and 2012Z. Unsurprisingly, these are 3/4 of the SNe Iax with the weakest narrow forbidden lines. Although a possible interpretation is that the narrow-component forbidden-line velocity shifts are poorly measured for these SNe, the narrow lines are clearly seen in SN 2008A. Another interpretation is that the physical regions producing the permitted and forbidden lines are essentially independent of each other for the SNe with strong broad forbidden lines.

Since the velocity shifts for the broad forbidden lines and permitted lines, even when there are no narrow P-Cygni features visible, are uncorrelated, it is likely that the mate-

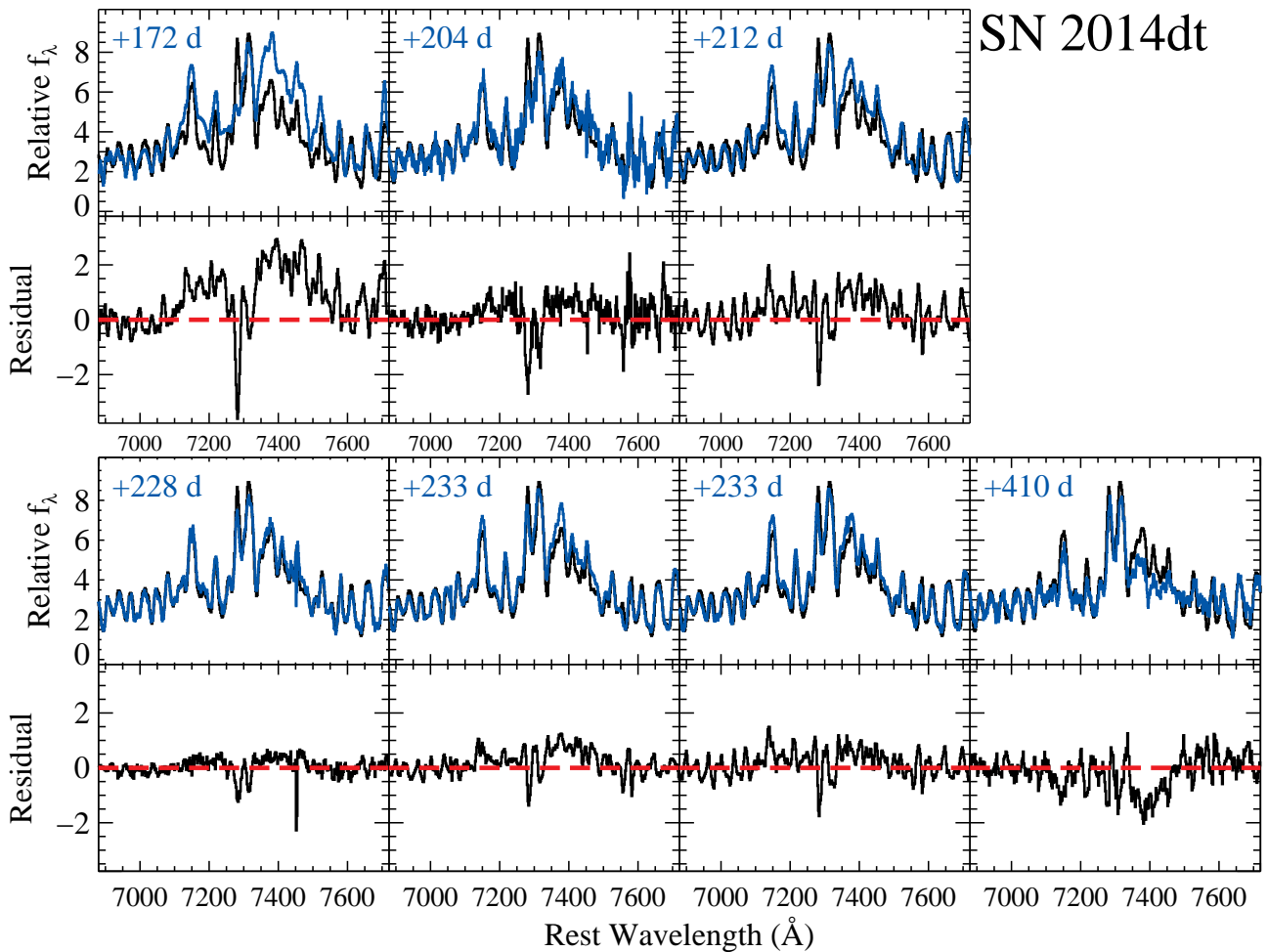


Figure 8. Late-time spectra of SN 2014dt from 172 to 270 d after maximum brightness, focusing on the forbidden-line region. The top panel of each row shows a different spectrum in blue, with its phase labeled. The +270 d spectrum is given in black for comparison in each subplot. The bottom panels of each row show the residual spectrum relative to the +270 d spectrum after they have been arbitrarily scaled to have their continua match just blueward and redward of the forbidden-line complex. The red dashed lines represent zero residual flux.

rial from which the broad forbidden lines are formed and the photosphere, which is where the continuum originates, are physically distinct. However, the correlation with the narrow forbidden lines and permitted lines suggests that those components *do* originate from the same material. These results favour the idea that late-time SNe Iax are composed of two physically distinct regions.

None the less, the photosphere and the material generating the broad forbidden lines are somehow connected. The SNe Iax with the broadest forbidden lines also lack distinct low-velocity P-Cygni features, suggesting that SNe Iax with higher-velocity photospheres also have higher-velocity, and more blueshifted, broad forbidden-line-forming regions.

3.5 Principal-component Analysis

To investigate the possibility that late-time SN Iax spectra have distinct physical components and to further examine correlations between spectral features, we perform a principal-component analysis (PCA) of the spectra. To do this, we subtract the average flux from each spectrum and

scale each spectrum to have a similar flux. We also shift the spectra in velocity space by their narrow forbidden emission line velocity shift. This last step reduces differences from small velocity shifts and focuses the analysis on differences in emission-line strengths and widths.

We present the first 5 eigenvalues for each SN in Table 2. Figure 9 displays the first 5 eigenspectra for our sample (all normalised to have the same maximum amplitude). The first 5 eigenspectra represent 40.8, 26.5, 11.0, 7.7, and 4.6% of the total variance between spectra, respectively. Cumulatively, this corresponds to 40.8, 67.3, 78.3, 85.9, and 90.5% of the total variance.

The eigenspectra show interesting correlations between features, including some correlations not identified in the previous sections. In the first eigenspectrum, the main features are broad components to the forbidden lines with anti-correlated narrow components. That is, the first eigenspectrum describes the relative strengths of the broad and narrow forbidden lines. Additionally, the first eigenspectrum also has a blue continuum correlated with stronger broad components. It is unclear if the colour difference is the re-

Table 2. Eigenvalues for Late-time SN Iax Spectra

| SN | 1st | 2nd | 3rd | 4th | 5th |
|--------|-------|------|------|-------|-------|
| 2002cx | 1.1 | 10.4 | 1.6 | -11.2 | -1.2 |
| 2005P | 15.7 | 18.3 | 12.9 | -3.6 | -9.9 |
| 2005hk | -9.2 | 23.0 | 33.1 | -0.6 | -1.2 |
| 2008A | 32.2 | 31.2 | 15.2 | 1.4 | -12.9 |
| 2008ge | 27.9 | 15.0 | 16.7 | 6.8 | -4.2 |
| 2010ae | -14.8 | 51.8 | 2.9 | 5.8 | -4.4 |
| 2011ay | 22.8 | 15.3 | 3.6 | 2.0 | -6.5 |
| 2011ce | -10.8 | -0.8 | 8.2 | 16.3 | -8.0 |
| 2012Z | 32.9 | 25.7 | 9.6 | 8.4 | 8.9 |
| 2014dt | 0.4 | 8.7 | 11.0 | -1.7 | 0.3 |

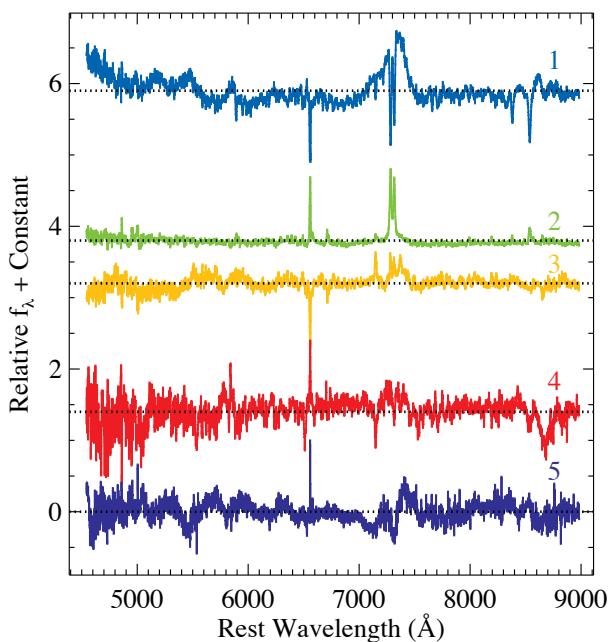


Figure 9. First five eigenspectra for late-time SN Iax spectra. The “zero flux” is annotated as a dotted line for each eigenspectrum.

sult of additional emission at these wavelengths or caused by (uncorrected) dust reddening (the latter is unlikely since the bluer continuum is correlated with narrow Na D absorption that is likely ISM absorption; intriguingly, we are unable to detect any narrow Na D within the broad Na D associated with the SN, but the eigenspectra are able to isolate this feature). Finally, the first eigenspectrum shows a correlation between high-frequency permitted lines and the strength of the narrow forbidden lines. Therefore, the first eigenspectrum suggests that SNe Iax with relatively strong narrow forbidden lines (and weaker broad forbidden lines) have more distinct permitted features.

The second eigenspectrum is basically a flat spectrum with mostly [Ca II] $\lambda\lambda 7291, 7324$ emission. This component is essentially uncorrelated with any other feature, although there is weak, narrow [Fe II] emission correlated with the [Ca II] emission. The continuum is slightly negative at nearly every wavelength, indicating that the overall continuum

strength is anticorrelated with the strength of the [Ca II] feature.

The third eigenspectrum has correlated narrow and broad forbidden lines that are anticorrelated with a blue continuum. This both confirms the necessity of broad and narrow forbidden lines and is a key discriminant for “transition” objects. The fourth eigenspectrum shows a correlation between narrow [Ni II] $\lambda 7155$ and broad Ca II NIR emission. The fifth eigenspectrum exhibits “P-Cygni-like” features for the broad emission lines, and is likely related to velocity shifts for the broad emission relative to the narrow emission.

Figure 10 displays the SNe 2002cx, 2008A, and 2008ge spectra (the same as in Figure 2) compared to their progressively reconstructed spectra. That is, the first comparison shows the first eigenspectrum multiplied by the first eigenvalue for that spectrum, while the second comparison shows that same projected spectrum added to the second eigenspectrum multiplied by the second eigenvalue for that spectrum. If there were zero variance beyond the fifth eigenspectrum, the final comparison would be equivalent to both the reconstructed spectrum and the true spectrum. For these spectra, a reconstruction using the first 5 eigenspectra results in reasonable reproductions of the data.

While the eigenvalues are representative of the projection of spectra onto the eigenvectors, the relative eigenvalues are more illustrative than their absolute values. Examining the eigenvalues for each spectrum, it is clear that the first eigenvalue is highly correlated with the strength of the broad forbidden lines, with SNe 2008A, 2008ge, 2011ay, and 2012Z having the largest (positive) eigenvalues and SNe 2005hk, 2010ae, and 2011ce having the smallest (negative) eigenvalues.

The second eigenvalues are positive for all SNe except for SN 2011ce. While one might naively think that the second eigenvalue dictates the strength of the observed [Ca II] emission, this is only partially correct. Spectra having large (positive) first eigenvalues also need large second eigenvalues to “fill in” the “absorption,” while negative first eigenvalues result in some [Ca II] emission, and so the size of the second eigenvalue is not perfectly correlated with the observed [Ca II] emission.

The second eigenvalue more directly tracks the continuum strength. For instance, the SNe with the largest second eigenvalue are SNe 2005hk, 2008A, 2010ae, and 2012Z, all of which have a small continuum level relative to their emission lines (see Figure 2). However, SNe 2002cx, 2011ce, and 2014dt, which have small second eigenvalues, all have relatively high continua relative to their emission lines.

The third eigenvalue provides some indication if a SN has a “transition” spectrum with both narrow and broad components. The SNe with the largest third eigenvalue, from strongest to weakest, are SNe 2005hk, 2008ge, 2008A, 2005P, and 2014dt. While not a direct correspondence, this group does include our previously identified transition objects and excludes the most extreme members of the class on both ends (e.g., SNe 2010ae and 2011ay).

Additional eigenspectra have more complicated interpretations. However, we caution against overinterpretation of the eigenspectra. The correlations, especially for less-significant eigenspectra, do not necessarily correspond to a physical cause and effect rather than simply correlation.

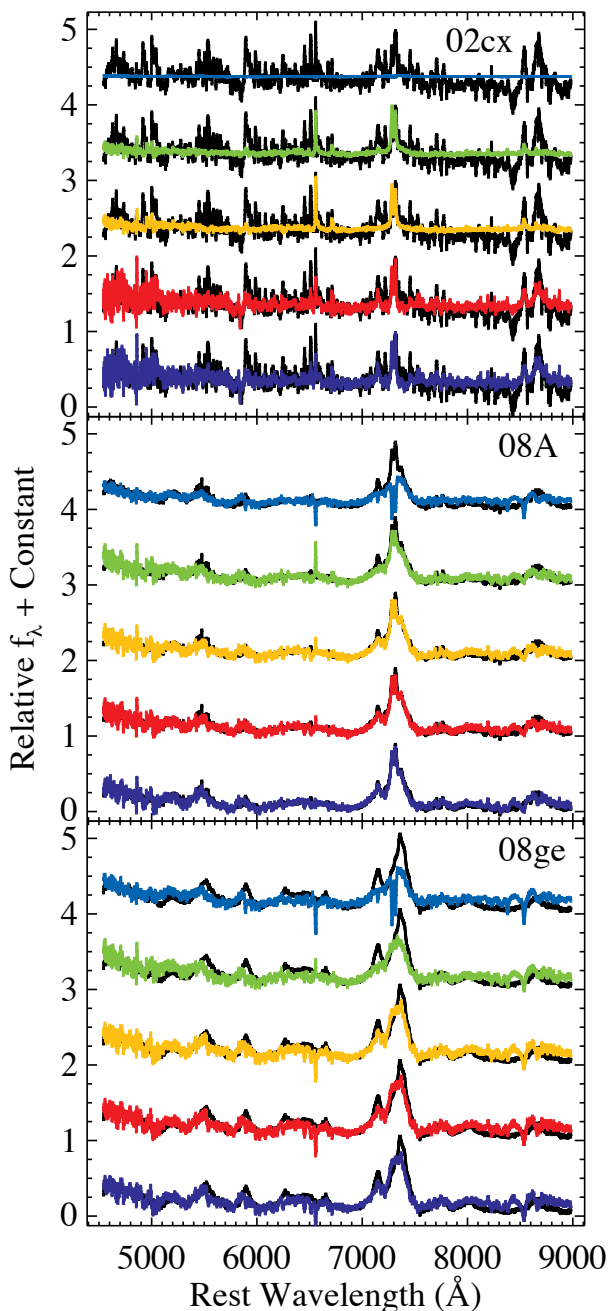


Figure 10. Late-time spectra of SNe 2002cx (top panel), 2008A (middle panel), and 2008ge (bottom panel) repeated in black. The successive (from top to bottom) coloured curves correspond to the reconstructed spectra using the first N eigenspectra, where N corresponds to the spectrum’s position from the top of the panel.

4 ANALYSIS

In Section 3, we described three different methods to examine the late-time ($t \gtrsim 200$ d) spectra of SNe Iax: model-fitting of forbidden lines, cross-correlation to determine velocity shifts, and a PCA. Here, we combine measurements from these methods along with other extant data to examine the causes of the spectroscopic diversity of SNe Iax at late times.

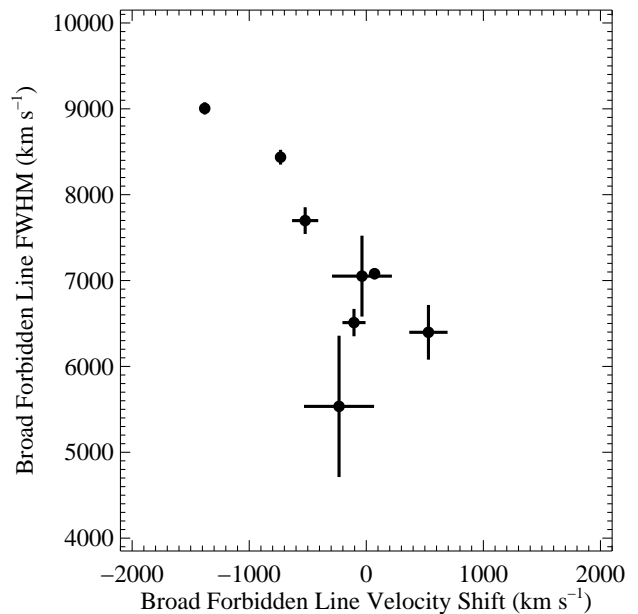


Figure 11. Line width as a function of velocity shifts for the broad forbidden-line components as fitted in Section 3.2. The correlation coefficient is -0.54 .

In addition to the velocity shifts, velocity widths, line strengths, line ratios, and eigenvalues derived above, we examine other SN properties as reported in other studies. In particular, we investigate the peak luminosity, the light-curve shape, and the photospheric velocity at maximum brightness.

4.1 Spectral Comparisons

We first examine the broad and narrow components of the forbidden lines individually. For the broad components, there is a strong correlation between the velocity shift and the velocity width (Figure 11; see also F13). Specifically, SNe Iax with blueshifted broad components tend to be broader than SNe with broad components that have no velocity shift or are redshifted. The correlation coefficient for this relation is -0.54 ; however, the true relation appears to be stronger than this number suggests. Performing a Bayesian Monte-Carlo linear regression on the data (Kelly 2007), we exclusively found non-negative slopes for the fitted lines in all of 200,000 trials, making the results significant at $>5.5 \sigma$.

More impressive is the relation between the EW of the broad [Ni II] $\lambda 7378$ emission and its velocity shift. These parameters are highly correlated: stronger lines correspond to more blueshifted lines. Figure 12 displays these two parameters, which have a correlation coefficient of -0.86 . A similar correlation is found with the broad [Fe II] $\lambda 7155$ emission, where the EW of that feature and its velocity shift have a correlation coefficient of -0.85 .

Six SNe Iax have blueshifted broad forbidden lines, while only two have redshifted lines (and two with no discernible broad component). Moreover, the redshifted objects are consistent with being at zero velocity (shifts of 70 ± 22 and 530 ± 160 km s^{-1} , respectively, with the uncertainties

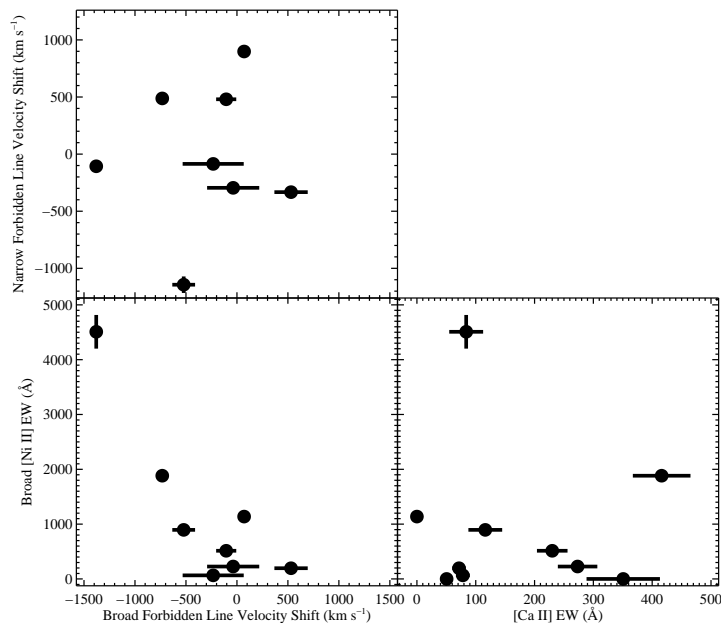


Figure 12. *Top-left:* Velocity shifts for the broad and narrow components of the forbidden lines as fitted in Section 3.2. The correlation coefficient is 0.20. *Bottom-left:* Broad [Ni II] $\lambda 7378$ EW as a function of its velocity shift as fitted in Section 3.2. The correlation coefficient is -0.83 . *Bottom-right:* Line strengths, relative to the continuum, for [Ca II] $\lambda\lambda 7291, 7324$ and broad [Ni II] $\lambda 7378$ as fitted in Section 3.2. The correlation coefficient is -0.06 .

not including typical galactic rotation of $200\text{--}300\text{ km s}^{-1}$). However, some SNe Iax appear to have truly blueshifted features (SNe 2008A and 2012Z). While this may be caused by chance (such a distribution has a $\sim 13\%$ chance of occurring), it is also possible that SNe Iax tend to have their broad nebular emission blueshifted or do not have broad emission at all.

This latter explanation is consistent with the correlation between width/strength and shift for these features. In this scenario, a weaker “broad” component will be narrower and less blueshifted. The extreme of this situation would be a “broad” component which is either too weak to be detected or too narrow to be distinguished from a separate “narrow” component.

We also examined the similar measurements for the narrow components. Here the correlation between line shift and width was not strong ($r = -0.17$). There may be some correlation for the narrow lines, but SNe 2008ge and 2011ay, which have the most blueshifted and redshifted lines (respectively), and thus highly influence any relation, pull the result in opposite directions. As both have weak narrow lines, either could be a systemic outlier, but it is currently impossible to determine if either is. Alternatively, the underlying physical relation may be between the magnitude of the shift (i.e., the absolute value) and the width of the line, for which there is a strong correlation ($r = 0.88$). With additional data, this relation should be re-examined.

Unsurprisingly, the strength of each individual broad/narrow component is (in general) highly correlated with each other. The strength of the two broad features have a correlation coefficient of 0.93, while the narrow [Fe II] and [Ni II] ([Ca II]) features have a correlation coefficient of 0.78 (0.46). The [Ca II] and narrow [Ni II] have a correlation coefficient of 0.61.

Next, we compare the properties of the broad and narrow components of the forbidden lines. As seen above, and especially as determined from the first eigenspectrum, the height of the (narrow) [Ca II] $\lambda\lambda 7291, 7324$ emission is anticorrelated with the height of the broad [Ni II] $\lambda 7378$ emission. While the heights of these features are moderately anticorrelated ($r = -0.52$), the EWs are uncorrelated ($r = -0.06$; Figure 12).

There is also no correlation between the velocity shifts of the narrow and broad components. Figure 12 compares these two values, showing no trend.

The broad and narrow components are generally uncorrelated. While there is some trend that SNe Iax with “stronger” [Ca II] emission have “weaker” broad [Ni II] emission, this is not seen in the EW measurements for these features. This may be partially caused by the anticorrelation between the continuum flux and [Ca II] emission (Section 3.5). Again, the lack of a strong connection between the broad and weak components indicates that they come from physically distinct components and perhaps physically distinct mechanisms.

Our physical interpretation of the eigenspectra in Section 3.5 is confirmed by comparing the eigenvalues of each spectrum to spectral parameters. For instance, the first and second eigenvalues predict the strength of the broad [Ni II] and narrow [Ca II] emission, respectively (Figure 13). As such, the eigenvalues can be used as a proxy for these values when it is difficult to measure them directly.

Finally, we compare the late-time spectral properties to those at maximum brightness. F13 presented maximum-light Si II $\lambda 6355$ velocities for SNe 2002cx, 2005hk, 2008A, 2011ay, and 2012Z. In addition, we use the spectrum of SN 2010ae presented by Foley (2013), which was obtained at $+0.8$ d, to measure a maximum-light velocity of $-4390 \pm$

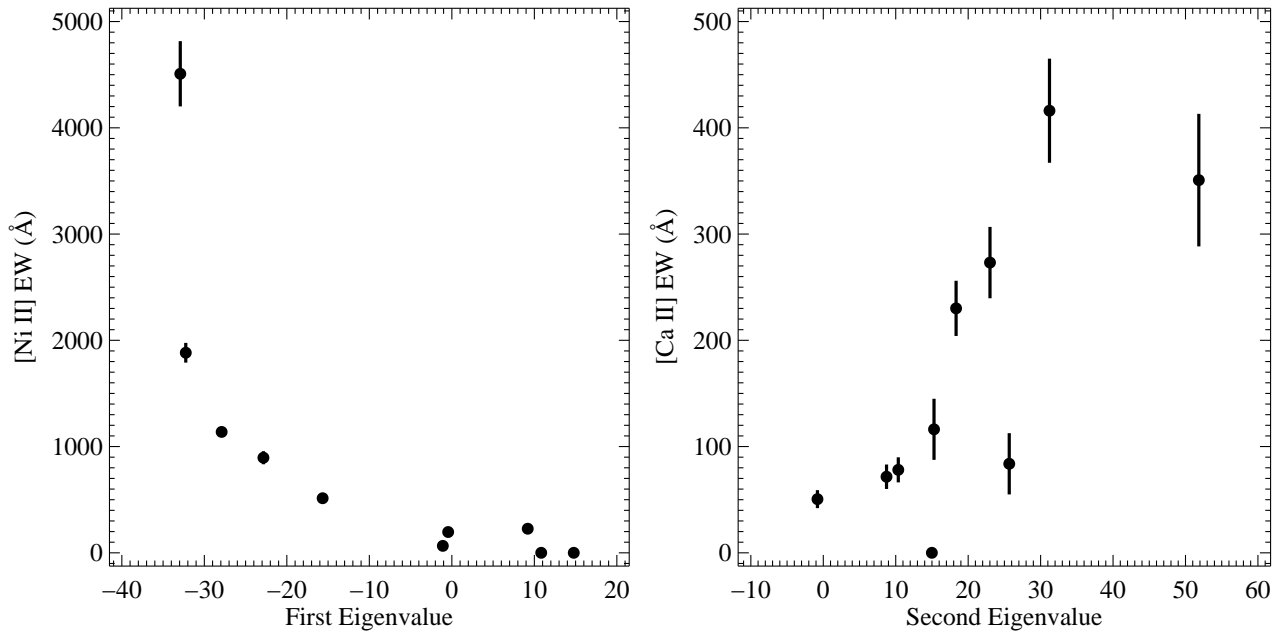


Figure 13. Broad [Ni II] $\lambda 7378$ (left) and narrow [Ca II] $\lambda\lambda 7291, 7324$ (right) EWs as a function of the first and second eigenvalues, respectively.

60 km s^{-1} . Therefore, six members of our sample have maximum-brightness measurements of their ejecta velocity.

While there is some correlation between maximum-brightness ejecta velocities and properties of the broad forbidden lines, the statistical significance (partially because SN 2010ae does not have a measured broad component) for any potential correlation is low.

However, the photospheric velocity is highly correlated ($r = 0.93$) with the first eigenspectrum (Figure 14). That is, the largest portion of the variance in the late-time spectra of SNe Iax is physically connected to the ejecta velocity at maximum brightness. Specifically, SNe with low measured ejecta velocities at maximum brightness tend to have late-time spectra with weak/absent broad forbidden lines and strong narrow [Ca II] lines.

4.2 Spectral–Photometric Comparisons

Using the subsample of SNe Iax that have both late-time spectra and photometric properties such as M_V and Δm_{15} , we examined potential correlations between the photometric properties and those derived from the late-time spectra.

There are no strong correlations between $\Delta m_{15}(V)$, the decline-rate parameter observed for most SNe Iax in our sample, and the appearance of the late-time spectra.

There is a strong correlation between the the peak absolute magnitude in the V band ($M_{V,\text{peak}}$) and both the velocity shift ($r = 0.83$; Figure 15) and width ($r = -0.85$) of the broad forbidden lines. While the first eigenvalue is also correlated with $M_{V,\text{peak}}$ ($r = 0.68$), it is not as highly correlated as the direct measurements of the broad forbidden lines. This is not caused by the addition of SN 2010ae (which was excluded from the previous comparisons because of a lack of an identifiable broad component); excluding SN 2010ae

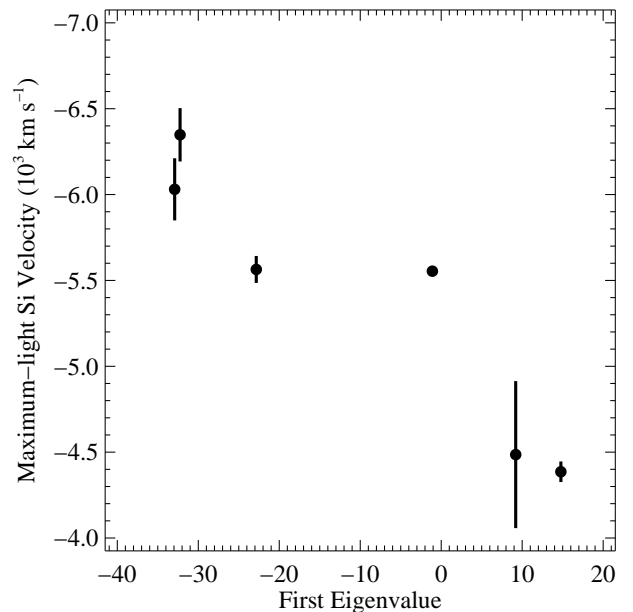


Figure 14. Comparison of maximum-light Si II $\lambda 6355$ velocity and first eigenspectrum of the late-time spectrum.

decreases the correlation between the first eigenvalue and $M_{V,\text{peak}}$ to $r = 0.51$.

The SNe Iax having higher peak luminosity tend to have broader, more blueshifted “broad” forbidden lines. Two possible explanations for this correlation are either (1) SNe Iax that produce more ^{56}Ni (and are thus more luminous at peak) also produce higher-velocity ejecta at all layers of the ejecta, or (2) SNe Iax explosions are asymmetric and lines

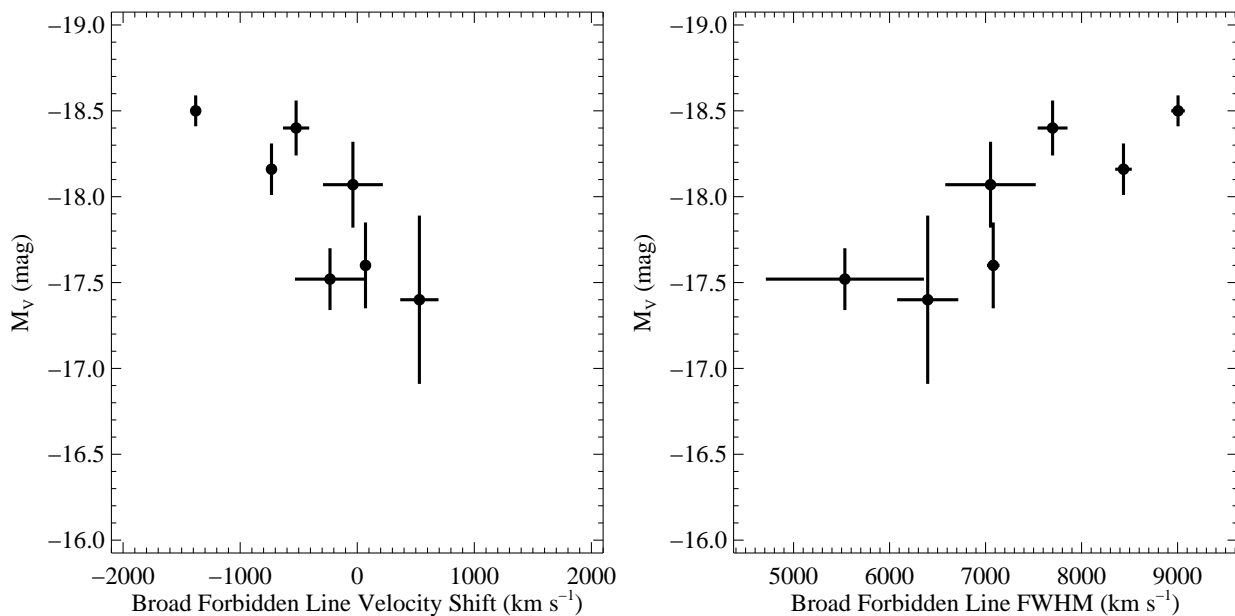


Figure 15. Peak absolute V magnitude as a function of velocity shifts (left) and velocity width (right) for the broad forbidden-line components as fitted in Section 3.2. The correlation coefficients are 0.83 and -0.85 , respectively.

of sight pointed along the “high-velocity axis” are also more luminous.

5 DISCUSSION

5.1 A Nearly Chandrasekhar-Mass Explosion

Our identification of the $[\text{Ni II}] \lambda 7378$ line in the late-time spectra of SNe Iax is a strong indication of the presence of stable nickel isotopes (e.g., ^{58}Ni) in the ejecta, as by >200 d after the explosion, radioactive ^{56}Ni will have decayed to a fraction $\sim 10^{-10}$ of its original abundance.

Explosion models which produce a deflagration flame that fails to unbind the progenitor WD³ can reproduce the rough spectral and photometric properties of SNe Iax (Jordan et al. 2012; Kromer et al. 2013, 2015). These models employ a (nearly) M_{Ch} WD progenitor. The burning is ignited in the core of this star, which has a sufficiently high density that electron capture produces neutronised isotopes such as ^{54}Fe and ^{58}Ni (e.g., Thielemann et al. 1986).

Contrastingly, detonations occurring in (or on) sub-Chandrasekhar WDs have densities too low for electron capture to occur. Although a small amount of ^{58}Ni may be synthesised using the excess neutrons from high-neutron species in the progenitor (primarily ^{22}Ne ; Timmes et al. 2003), it is expected that the amount of ^{58}Ni is significantly less than that of all Fe species in such explosions.

While detailed nebular spectrum calculations are needed to infer the nickel and iron abundances, the detection of strong $[\text{Ni II}]$, especially being much stronger than $[\text{Fe II}]$, can be interpreted as strong evidence for a (nearly) M_{Ch} progenitor star. Accordingly, this is further support for

the deflagration models which fail to unbind their progenitor star.

If the progenitor stars at the time of explosion have masses of $1M_{\odot} \lesssim M \lesssim M_{\text{Ch}}$, and in particular if they are close to the Chandrasekhar mass, then the implied ejecta masses of $\sim 0.5 M_{\odot}$ (or less) for most SNe Iax (see, e.g., Foley et al. 2010b, 2013; Narayan et al. 2011; McCully et al. 2014b) require a bound remnant for nearly all SNe Iax.

5.2 Size of the Late-time Photosphere

At late times ($t \gtrsim 200$ d), some SNe Iax still have permitted lines with P-Cygni features, indicative of persistent photospheres (J06). Although we cannot detect individual P-Cygni features for some SNe Iax, the continua of all SNe Iax are similar. Additionally, the bluer $[\text{Fe II}]$ and $[\text{Fe III}]$ features seen in late-time spectra of SNe Ia are absent in all late-time SN Iax spectra. It is therefore likely that all SNe Iax have a photosphere at late times.

We can measure the size of the photosphere in two independent ways. The first is to measure the luminosity and temperature of a SN Iax at late times and determine the radius assuming that the emission comes from a blackbody. The second is to assume that the velocity of the late-time P-Cygni lines is characteristic of the velocity of the late-time photosphere. Assuming no acceleration, one can measure the radius knowing the time between explosion and the time of the spectrum.

For these measurements, we will emphasise the well-observed SN 2005hk (Phillips et al. 2007; Sahu et al. 2008; McCully et al. 2014b), focusing on the +402 d spectrum (417 days after explosion) presented by Silverman et al. (2012). This is the last spectrum of SN 2005hk which still has a clear continuum. At this time, the bolometric luminosity of SN 2005hk was $\sim 10^{39.9}$ erg s⁻¹ (McCully et al. 2014b). The bolometric luminosity was determined from broad-band

³ These models are sometimes referred to as “failed deflagration” models, despite the fact that the deflagration is successful.

photometry, and may overestimate the continuum flux by as much as 40% because of line emission (as determined from the optical spectrum). Fitting a blackbody spectrum to the continuum of SN 2005hk at this epoch, we find a best-fitting temperature of $\sim 4500 - 5500$ K, consistent with the presence of both Fe I and Fe II in the spectrum (Hatano et al. 1999; McCully et al. 2014b). Using the above values, we determine that the blackbody radius 417 d after explosion is

$$R_{\text{BB}} = 1.3 \times 10^{14} \left(\frac{L}{10^{39.9} \text{ erg}} \right)^{1/2} \left(\frac{T}{5000 \text{ K}} \right)^{-2} \text{ cm.} \quad (1)$$

The uncertainty in the radius measurement is $\sim 20\%$ given the uncertainties in the luminosity and temperature, and the range in radius is the result of different assumptions about the continuum luminosity and blackbody temperature.

The +402 d spectrum of SN 2005hk has a photospheric velocity (as determined from the P-Cygni absorption) of -410 km s^{-1} , similar to what was found for SN 2002cx at late times (Jha et al. 2006). If the emitting material for SN 2005hk has been in homologous expansion since explosion, this would place the material at

$$R_{\text{kin}} = 1.5 \times 10^{15} \left(\frac{v}{410 \text{ km s}^{-1}} \right) \left(\frac{t}{417 \text{ d}} \right) \text{ cm,} \quad (2)$$

a radius more than an order of magnitude *higher* than the blackbody radius. The uncertainty in this measurement is around 2% and primarily set by the uncertainty in the measured velocity.

These two discrepant estimates of the photospheric radius cannot be reconciled by any simple adjustment of the measured quantities. First, the late-time photospheric velocity would need to be overestimated such that the true velocity is $v_{\text{ph}} \lesssim 40 \text{ km s}^{-1}$, which is much too low to be consistent with the spectrum. Alternatively, the bolometric luminosity could be $\sim 10^{42} \text{ erg s}^{-1}$, which is >2 orders of magnitude higher than measured. Finally, a true temperature of 2500 K would sufficiently reduce the measured blackbody radius; however, at this temperature, we would not expect to see any Fe II emission. Furthermore, such a low temperature would require that the continuum seen in the spectra be caused by a nonblackbody component, making our luminosity assumption incorrect — a lower blackbody luminosity with this lower temperature is similarly inconsistent with the kinematic radius. In summary, it does not appear that a poor assumption or measurement error has resulted in this discrepancy.

Another possible explanation for the different radius estimates is asymmetry, but this ultimately seems unlikely. The kinematic radius describes the radius along the line of sight, while the blackbody radius describes the (average) radius in the plane of the sky. A highly asymmetric explosion could thus have very different measurements for the radius. However, this would require an extreme aspect ratio and very particular viewing angle. This becomes even less likely considering the number of other SNe Iax similar to SN 2005hk and the lack of strong polarization at early times for SN 2005hk (Chornock et al. 2006; Maund et al. 2010).

Alternatively, the photospheric material may not have been expanding since the time of explosion. If the material generating the photosphere were launched at 410 km s^{-1} 30–40 d before the time of the spectrum (with a shorter period if

there is deceleration), this would place the kinematic radius at the same radius as the blackbody radius. However, in this scenario, the material would not be caused by the initial explosion and must be a wind from either the companion star or a surviving remnant.

In the case of a wind, the velocity of the photosphere should be essentially the wind velocity; the SN explosion would have created a cavity and so there would be minimal deceleration. (However, if there is a bound remnant, there may be infalling material even at late times which could decelerate the wind.) Assuming that the photosphere seen at late times for SN 2005hk is the result of a 410 km s^{-1} wind, equivalent to the escape speed of a compact remnant, this remnant would have a radius at late times of $R = 8 \times 10^{10} (M/0.5M_{\odot}) \text{ cm} = 1.2 (M/0.5M_{\odot}) R_{\odot}$. For this scenario, the mass-loss rate would need to be high enough such that the wind remains optically thick out to a radius of $\sim 10^{14} \text{ cm}$, or $\sim 10^3 R_{\odot}$.

The velocity of the permitted lines seen in the SN 2005hk spectra decreased by $\sim 100 \text{ km s}^{-1}$ between 245 d and 417 d after explosion, corresponding to $\sim 0.5 \text{ km s}^{-1} \text{ d}^{-1}$. This incredibly slow change in the photospheric velocity is also difficult to explain with a single homologous expansion, thus favouring a wind interpretation.

5.3 A Two-Component Ejecta Model

The above radius estimates argue for a late-time wind from the progenitor system. Explosion models which match the early-time spectra and light curves of SNe Iax also argue for a bound remnant (Jordan et al. 2012; Kromer et al. 2013, 2015). These models predict that a significant amount ($\sim 0.02 M_{\odot}$) of ^{56}Ni will remain in the remnant, providing an energy source that may be able to drive dynamical outflows. It is reasonable to think that after a SN Iax explosion a bound remnant would expand to $R \approx R_{\odot}$ and drive a super-Eddington wind (Bildsten et al., in prep.). This model also solves the problem of having low-velocity material from an explosion that completely disrupted the star (McCully et al. 2014b).

However, for our observations, we do not require that the wind comes from a bound remnant. Rather, the wind could be caused by the remnant or the companion star. While it is not yet possible to distinguish between these two possibilities, the significant ^{56}Ni in the bound remnant would be a natural energy source to drive such a wind.

In the wind scenario, the photosphere is significantly smaller than the forbidden-line emitting region, which is likely dominated by SN ejecta. For the case of SN 2005hk, assuming that nearly all of the luminosity comes from the photosphere at late times, the photosphere was at $R \approx 10^{14} \text{ cm}$ at +402 d, while the forbidden-line emitting region should be at

$$R_{\text{ej}} \approx 1.3 \times 10^{16} \left(\frac{v}{3500 \text{ km s}^{-1}} \right) \left(\frac{t}{417 \text{ d}} \right) \text{ cm,} \quad (3)$$

where the velocity is given by the half width at half-maximum intensity (HWHM) of the broad forbidden lines. At this radius, the forbidden-line emitting region has a radius about 100 times larger than the photosphere, and thus the projected area of the forbidden-line region is $\sim 10^4$ times larger than that of the photosphere. Even in the case

where the material creating the photosphere (moving at $\sim 500 \text{ km s}^{-1}$) was ejected at the same time as the higher-velocity material, the forbidden-line emitting region will be ~ 75 times larger than the photosphere in projected area. In either case, the photosphere cannot block a significant amount of the forbidden-line region, and the forbidden lines must track essentially all of the low-density material, with very little blocked by the photosphere.

Beyond the optically thick region of the wind, lower-density wind material may generate the narrow forbidden lines. For a constant-velocity wind, unlike a homologous flow, the material at larger radius would share the same velocity as the photospheric material. The HWHM of the narrow forbidden components is typically $\sim 500 \text{ km s}^{-1}$, although SNe with detected narrow P-Cygni features (e.g., SNe 2002cx and 2005hk) tend to have slightly narrower forbidden lines (HWHM $\approx 400 \text{ km s}^{-1}$). These velocities are consistent with a $\sim 500 \text{ km s}^{-1}$ wind. The gradual, correlated change in the velocities for the permitted and narrow forbidden lines between +230 d and +403 d for SN 2005hk implies that the two are physically connected, again supporting the idea that the narrow forbidden lines are linked to a wind that is producing the photosphere and low-velocity P-Cygni features. Even the large widths seen in some spectra could be consistent with a wind if the remnant has a smaller radius or larger mass (and thus larger escape velocity).

The distribution of narrow-line velocity shifts peaking at zero velocity and the lack of a correlation between the narrow and broad components are all consistent with the narrow-line regions being formed by a wind. Similarly, the lack of broad Ca lines may be indicative of different compositions for the broad and narrow components. The compositional difference is a natural outcome of the narrow and broad lines originating from a remnant wind and the SN ejecta, respectively. For instance, the model of Kromer et al. (2013) has the remnant composed of 88% C/O and 3% iron-group elements (IGEs), while the ejecta are only 28% C/O and 59% IGEs. While this model may not perfectly match the relative abundances of the ejecta and wind (especially since the wind will be composed of surface material), the model may predict strong, narrow [O I] $\lambda\lambda 6300, 6364$ emission. However, strong [O I] has not yet been observed in a SN Iax (J06; McCully et al. 2014b), and since both [Ca II] and Ca II are seen in the spectra, the density is sufficiently high to suppress [O I] emission (McCully et al. 2014b). None the less, this potential compositional difference may explain the lack of broad [Ca II] lines. The Kromer et al. (2013) model has 9.7 and 220 times as much (by mass) IGEs as Ca in the remnant and SN ejecta, respectively. This difference is generally consistent with having relatively strong/absent narrow/broad Ca lines.

If the narrow forbidden lines are indicative of a wind, then nearly every SN Iax must have such a wind. With the possible exception of SN 2011ay, which does not have an obviously distinct low-velocity component, all SNe Iax in our sample have some narrow lines.

There is significant diversity in the strength, width, and velocity shifts of the broad component of the forbidden lines. These properties are strongly correlated with maximum-light properties such as peak luminosity, but uncorrelated (or weakly correlated) with the narrow forbidden lines, indicating two distinct kinematic components.

In the wind model, the narrow forbidden lines, the low-velocity P-Cygni lines, and the photosphere would be generated by a wind, while the broad forbidden lines would be related to the SN ejecta, and thus to early-time SN properties.

Kromer et al. (2013) modeled SN 2005hk with such a two-component model and were able to separate the SN luminosity from the luminosity of the bound remnant. In this model, the ejecta of SN 2005hk should have a luminosity of roughly $10^{39.3} \text{ erg s}^{-1}$ at the time of the late-time spectrum analyzed above (time since explosion of ~ 417 d). This is roughly 20% of the total bolometric luminosity. Examining the SN 2005hk spectra, we find that the broad forbidden lines discussed in this work represent $\sim 5\%$ of the optical luminosity. For the SN 2012Z spectrum analyzed above, which had the strongest broad absorption lines of our sample, the broad forbidden lines represent $\sim 45\%$ of the total optical luminosity at late times. Therefore, the broad forbidden lines, which one would naturally associate with the SN emission, have roughly the predicted fractional flux of the SN ejecta in the Kromer et al. (2013) model.

In this two-component ejecta model, where one component is from the SN explosion and the other is from the wind, there is not necessarily any direct physical connection between the two components. That is, the amount of ^{56}Ni left in the remnant and the mass of the remnant, which must be the primary variables for the strength of the wind and its velocity, may be essentially unrelated to the amount of ^{56}Ni ejected and the ejecta mass, which are likely the primary variables for SN properties. While a “stronger” explosion is expected to produce more ^{56}Ni , it is unclear what percentage of the progenitor star is burned, what the initial mass of the progenitor star is, or what fraction of ^{56}Ni is ejected relative to that left in the remnant.

Kromer et al. (2015) produced a model explosion that roughly matches the observed properties of SN 2008ha (Foley et al. 2009, 2010b; Valenti et al. 2009), the least-luminous SN Iax yet discovered. While the Kromer et al. (2013) model used a C/O WD progenitor, the Kromer et al. (2015) model used a hybrid C/O-Ne WD. The composition of the WD accounts for the different outcomes; however, the exact ignition conditions could affect the mass burned in the deflagration. While SN 2008ha was not detected at late times (Foley et al. 2010b), this model may provide insight into the diversity of ejecta for SNe Iax having different luminosities. In this model, 46% of the ejecta is composed of IGEs, lower than for the Kromer et al. (2013) SN Iax model, indicating a possible compositional difference for low- and high-luminosity SNe Iax.

Using these two models as examples, there is a trend between peak luminosity and ejecta mass. The Kromer et al. (2013) and Kromer et al. (2015) models have peak V -band absolute magnitudes of -18.2 and -14.8 , respectively (and a factor of 23 in luminosity), while they also produce 0.372 and $0.014 M_{\odot}$ of ejecta, respectively (a factor of 27). Based on these models, one may expect that peak luminosity is related to the relative strength of the broad forbidden-line emission, which would have some dependence on ejecta mass.

To examine this possibility, Figure 16 displays the correlation between $M_{V, \text{peak}}$ and broad-component [Ni II] $\lambda 7378$ EW. There is a modest correlation (correlation coefficient of -0.53), where more-luminous SNe Iax tend to have stronger

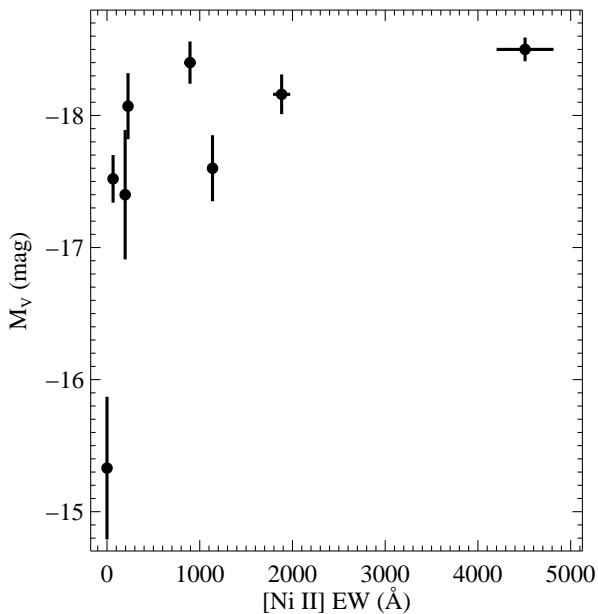


Figure 16. Peak absolute V magnitude as a function of the broad-component [Ni II] $\lambda 7378$ EW. The correlation coefficient is -0.53 .

broad emission lines. However, there is no correlation between the narrow-component [Ni II] $\lambda 7378$ EW and peak luminosity ($r = -0.15$), consistent with a wind that is relatively independent of the SN ejecta.

5.4 An Asymmetric Explosion?

The two-component model described above is insufficient for reproducing the correlation between peak luminosity and velocity shifts of the broad forbidden-line emitting region (i.e., Figure 15). That model also does not explain the predominantly blueshifted broad forbidden lines regardless of any correlation with peak luminosity.

The latter is difficult to explain with a simple two-component model. For a predominantly blueshifted population, one would expect that the redshifted emission be blocked by a photosphere. However, above we found that the broad forbidden-line emitting region is $\sim 10,000$ times larger than the photosphere (in projection) at ~ 417 d after explosion. Even for the typical phases of the spectra analyzed in this work, the broad forbidden-line emitting region is likely ~ 3000 times larger than the photosphere. In this scenario, the photosphere would be unable to block most of the redshifted emission.

If we require a photosphere to block the redshifted emission of the broad forbidden-line emitting region, it should have a projected area $\lesssim 10\times$ that of the area of the photosphere. One scenario is that the SNe with blueshifted forbidden lines also have much larger photospheres ($\gtrsim 2 \times 10^{15}$ cm) than that of SN 2005hk. This photosphere, if at ~ 5000 K, would have a large luminosity of $\sim 10^{42}$ erg s^{-1} . This is much larger than any SN Iax measured at late times (e.g., McCully et al. 2014b) and not significantly less than the peak SN luminosity.

Alternatively, the broad emission, which should come

from the SN ejecta, may not be distributed symmetrically. In fact, reasonable explosion models expect few plumes, which could result in highly asymmetric ejecta (Jordan et al. 2012; Kromer et al. 2013). If, for instance, there is higher-velocity material ejected primarily along a single axis, then when we see a large velocity, corresponding to a line of sight along this axis, a smaller photosphere could block the redshifted emission. Correspondingly, looking perpendicular to this axis would result in no broad lines. This is an intriguing model to describe the diversity of SN Iax late-time spectra, including the transition objects, which would be viewed at an angle intermediate to the two examples mentioned above.

A downside of this model is that one would predict extremely large asymmetries in the SN ejecta and thus large polarization, which is inconsistent with measurements made for a single SN Iax, SN 2005hk (Chornock et al. 2006; Maund et al. 2010). However, the photosphere at the times of polarization measurements might not have been dominated by this asymmetric material or SN 2005hk may be an atypical object. In fact, it may be the case that the blueshifted objects come from a subpopulation that have strong asymmetries, while other SN Iax explosions are more spherical. Additional spectropolarimetric observations of SNe Iax, and comparisons to other spectral and photometric properties, will test this possibility.

5.5 The “Late-time” SN 2008ha Spectra

SN 2008ha is an exceptional SN Iax, being the least luminous member of the class ($M_{V,\text{peak}} = -14.2$ mag; Foley et al. 2009; Valenti et al. 2009), fading very quickly ($\Delta m_{15}(B) = 2.2$ mag; Foley et al. 2009), and having very low-velocity ejecta at peak brightness ($v_{\text{ph}} = -3700$ km s^{-1} ; Foley et al. 2010b). Combined, the data suggest that the SN ejected $M \lesssim 0.3 M_{\odot}$ (Foley et al. 2010b), significantly less than that expected for a WD SN that completely unbinds its star. Intriguingly, at $t \approx +4$ yr, there is a very red star detected in *HST* images coincident with the position of SN 2008ha (Foley et al. 2014). While this may be a chance coincidence, it is also possibly the surviving remnant of the WD.

For all of these reasons, SN 2008ha appears to be an extremely interesting object for testing the wind model. Unfortunately, the only late-time spectrum of SN 2008ha, at $t = +231$ d, did not reveal any SN emission (Foley et al. 2010b). Therefore, the latest spectroscopic data for SN 2008ha extend to only ~ 2 months after peak (Foley et al. 2009; Valenti et al. 2009). However, even at these early times, the spectrum exhibited strong [Ca II] emission (Foley et al. 2009; Valenti et al. 2009).

For the first time here, we note that for phases of $t \gtrsim +37$ d, the spectra of SN 2008ha look remarkably similar to those of other SNe Iax at $t > 200$ d. Specifically, SN 2008ha has emission from [Ca II], [Fe II], and [Ni II] starting around a month after peak brightness. We detect this emission in the +37 d spectrum, but it is absent in the +22 d spectrum.

We compare the +37 d and +63 d spectra of SN 2008ha to the +227 d spectrum of SN 2002cx in Figure 17. The continua and permitted lines in the spectra of the two SNe are nearly identical. The primary difference is the strength of the forbidden lines. At +37 d, SN 2008ha has relatively stronger [Ca II] and weaker [Fe II] and [Ni II] than SN 2002cx. However, at +63 d, SN 2008ha has [Ca II] emission that is

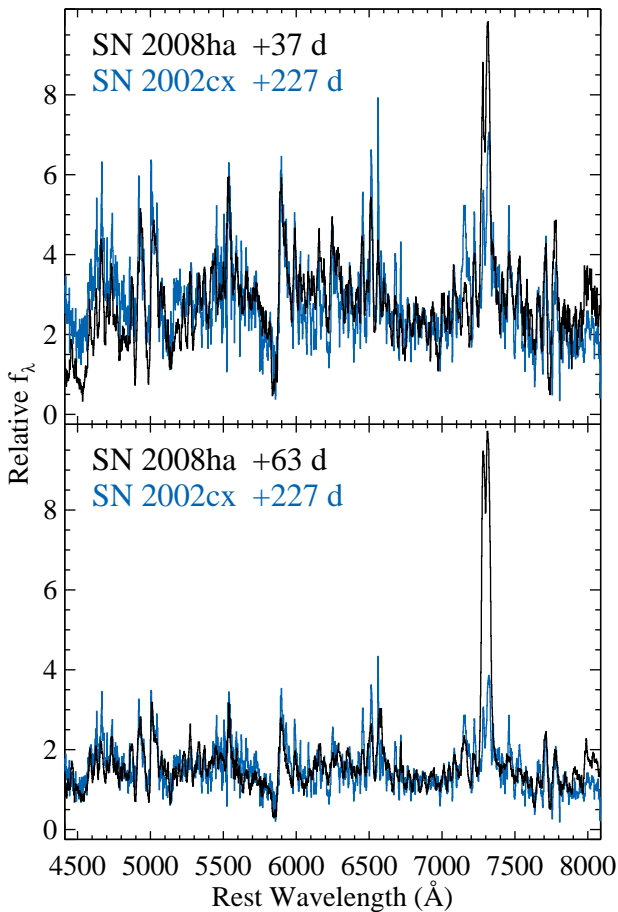


Figure 17. Optical spectra of SN 2008ha (black curves; top panel is at $t = +37$ d; bottom panel is at $t = +63$ d) and SN 2002cx (blue curves; $t = +227$ d). The spectra are remarkably similar despite their very different phases.

roughly 10 times as strong as for SN 2002cx (relative to the continuum emission). At this time, the [Fe II] and [Ni II] emission is similar in the two objects (again, relative to the continuum).

From spectra alone, it appears that SN 2008ha has a “late-time” appearance starting only ~ 1 month after peak. This is exceptionally fast evolution. If our wind model is correct, we would expect the wind to be launched before ~ 50 d after explosion (since SN 2008ha had a rise time of ~ 10 d), placing a strong lower limit to this condition in at least the lowest-luminosity SNe Iax. Regardless, it appears that SN 2008ha transitioned to have “late-time” behaviour at an incredibly early time.

The Kromer et al. (2015) model for SN 2008ha resulted in six times as much ^{56}Ni in the bound remnant than in the SN ejecta. As a result, the instantaneous energy deposition is always larger for the remnant than in the ejecta. Depending on the distribution of ^{56}Ni in the remnant, one could imagine the wind being the dominant component at these early times.

We also examined the spectra of SN 2010ae, another low-luminosity, low-velocity SN Iax (Stritzinger et al. 2014). Despite the other similarities to SN 2008ha, SN 2010ae does not exhibit any forbidden emission through +57 d. There

are no published spectra of SN 2010ae between +57 d and +252 d (we examine this late-time spectrum above); therefore, we cannot assess if SN 2010ae transitioned to having a “late-time” spectrum at a relatively early time. None the less, we can definitively say that this transition happened later in SN 2010ae than in SN 2008ha.

Finally, while the >1 month SN 2008ha spectra are extremely similar to those of SNe Iax at >6 months, we have chosen to not include these spectra in the other analysis presented here so as to examine only SNe Iax at late times rather than select objects based solely on spectral similarities.

5.6 Lack of Dust in SN 2014dt

Fox et al. (2015) detected SN 2014dt as a relatively strong IR source at phases of +302 to +329 d after peak brightness. The IR flux was interpreted as dust emission either from pre-existing circumstellar dust or dust newly formed in the SN ejecta. Fitting the two IR bands, they infer a dust mass of $\sim 5 \times 10^{-6} M_{\odot}$ (using our preferred distance) and a blackbody temperature of 700 K. Fox et al. (2015) measure an increase in IR luminosity during this month of observations, and while this is only significant at $\sim 1 \sigma$, it may be indicative of an increasing luminosity of an IR-bright component to SN 2014dt.

As noted by Foley et al. (2015) and Fox et al. (2015), there is no indication of dust reddening for SN 2014dt at early times. Fox et al. (2015) notes that SN 2014dt becomes redder (in $B - V$) at ~ 250 d after peak. This claim is based on a single data point that is discrepant from other SN Iax colour curves at $\sim 3 \sigma$. However, there is some indication of SN 2014dt becoming redder at these times in our late-time spectra. Fox et al. (2015) interpret the change in colour as coming from additional flux of a redder component and not new dust reddening. Using the light-curve data presented by Fox et al. (2015), including the extrapolated optical light curves, we find that based on the IR luminosity, a 2000 K blackbody can contribute at most 0.3% of the V -band flux, with lower temperatures contributing even less flux. Therefore, it is unlikely that a single blackbody can both account for the IR flux and change the $B - V$ colour.

Given the low reddening at early times, it is unlikely that there was any significant amount of pre-existing circumstellar dust. There are also strong limits on narrow absorption lines in the spectra of SN 2014dt (Foley et al. 2015), indicating a gas-poor circumstellar environment. Furthermore, there is no indication of any circumstellar interaction in any spectra (Figure 1), including the +410-day spectrum (Figure 18). The circumstellar dust scenario seems unlikely given existing data.

We can also test the possibility of newly formed dust with data presented here. Dust can form in the SN ejecta, and this will redden the SN, produce an IR excess, and preferentially extinguish the redshifted light in forbidden lines (e.g., Smith et al. 2008). With our +410-day spectrum of SN 2014dt, which was obtained after the IR data, we can rule out any significant newly formed dust.

Most obviously, there are no clear changes to the forbidden-line shapes. Figure 18 displays the late-time spectra of SN 2014dt from +270 d and +410 d. While there is a slight change in the strength of the [Ni II] emission (see Sec-

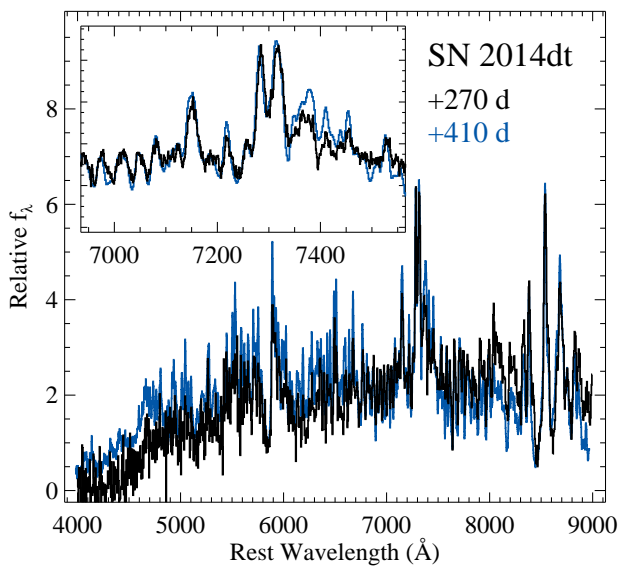


Figure 18. Late-time spectra of SN 2014dt at phases of roughly +270 d (black curve) and +410 d (blue curve). The spectra are very similar. The slight difference in continuum shape is inconsistent with dust reddening, but is consistent with slightly different photospheric temperatures. There is no indication for circumstellar interaction in either spectrum. *Inset:* Zoom-in of the region near the forbidden emission lines. There is no indication of preferential extinction for the red side of the forbidden-line profiles.

tion 3.3), the forbidden lines are otherwise nearly identical in strength, width, velocity shift, and profile. In particular, there is no preferential extinction of redshifted material. This is consistent for all spectra of SN 2014dt, including the +410 d spectrum, which was taken after the IR observations.

Additionally, there is no obvious emission from a warm, ~ 2000 K (corresponding to the dust deposition temperature) blackbody (see Figure 1) as was seen for the dust-forming SN 2006jc (Smith et al. 2008). However, given the IR luminosity, such a component is not necessarily expected. None the less, this is further indication that the change in $B - V$ colour is intrinsic to the SN and not a result of an additional blackbody component.

Examining the wavelength regions near hydrogen Balmer, He I, and He II lines, we see no indication of narrow emission as would be expected from circumstellar interaction. While this does not rule out the presence of circumstellar material, it does constrain the amount of such matter and the mechanism for heating potential circumstellar dust.

Finally, there is no indication of additional reddening. While the continuum of SN 2014dt has slowly become redder with time, we are unable to deredden later spectra to match earlier spectra using normal reddening laws and reasonable reddening parameters. While one can deredden later spectra to roughly match the continuum at either bluer or redder wavelengths, it is not possible to adequately match all wavelengths simultaneously. Moreover, such a manipulation changes the strengths of the spectral features. While all observed spectra have roughly similar line strengths from +172 to +410 d, dereddening spectra causes bluer lines to become relatively stronger and redder lines to become relatively weaker. For the SN to have additional reddening, it

must be a particularly odd reddening law and the SN spectral features must evolve in a way to perfectly counteract the effects of reddening. We find this behaviour to be highly unlikely.

An alternative explanation for the IR emission in SN 2014dt, which was not explored by Fox et al. (2015), is that it comes from a bound remnant with a super-Eddington wind. Such a mechanism is consistent with the SN 2014dt data, late-time data for all SNe Iax, and the potential counterpart seen for SN 2008ha (Foley et al. 2014). Considering the lack of any obvious circumstellar material or dust, as well as the observed long-lasting photosphere and low photospheric velocities, the best model for the IR emission is that it is somehow related to the bound remnant, and most likely as an optically thick super-Eddington wind.

6 CONCLUSIONS

We have presented an analysis of the late-time spectra of a sample of 10 SNe Iax. We add 8 spectra of SN 2014dt, the closest SN Iax yet discovered, to literature data to form our dataset. We find that while there are some subtle changes to the spectra at $t \gtrsim 200$ d after peak brightness, a single late-time spectrum is generally sufficient to describe the late-time behaviour of a SN Iax. In particular, we find SNe Iax to be in a continuum between two extremes: (1) those having low-velocity (~ 500 km s $^{-1}$) permitted P-Cygni lines and strong/narrow forbidden [Fe II], [Ni II], and [Ca II], and weak (or absent)/broad [Fe II] and [Ni II]; and (2) those having relatively smooth continuum emission with a shape similar to that of other SNe Iax, relatively weak (perhaps even absent in one case)/narrow forbidden [Fe II], [Ni II], and [Ca II], and strong/broad [Fe II] and [Ni II].

By fitting the forbidden lines, cross-correlating the spectra, and performing a PCA, we have quantitatively shown that the spectral continuum described above is real, with the various correlated properties listed being significant. We further note that besides the relative strength of the narrow/broad forbidden lines, the two kinematic components appear to be physically disconnected. That is, the velocity shifts and widths of the broad and narrow components are uncorrelated.

We find a strong correlation between the width/strength of the broad forbidden lines and their blueshift. We also find no SNe Iax that have clearly redshifted broad forbidden lines, while there are several that are significantly blueshifted. It is unclear if this trend is simply a result of a relatively small sample.

We find that SNe Iax that have higher ejecta velocities measured at maximum brightness also have stronger broad forbidden lines. This can be explained if explosions with higher kinetic energy per unit mass also eject more material. We also find that the more luminous (at peak) SNe Iax have stronger, broader, and more blueshifted broad forbidden lines. This requires that either SNe Iax that produce more ^{56}Ni (in their ejecta) also have higher-velocity ejecta, or that SNe Iax are highly asymmetric and lines of sight that see higher-velocity ejecta are also more luminous. Such claims can be tested in the future with additional spectropolarimetry of SNe Iax.

The strong [Ni II] lines in SN Iax spectra at >200 d af-

ter explosion must come from stable Ni, presumably ^{58}Ni . Producing such a large amount of stable Ni requires electron capture, which can only occur at the high densities of a (nearly) M_{Ch} WD. Although full nebular modeling is necessary to confirm the Ni (and Fe) abundances, this is further support for the idea that deflagrations of (nearly) M_{Ch} WDs that fail to unbind their stars produce SNe Iax (Jordan et al. 2012; Kromer et al. 2013, 2015).

We found that the kinematic radius of SN 2005hk (determined from the velocity of the photosphere at late times and the time since explosion) is an order of magnitude higher than the blackbody radius (determined from the luminosity and temperature). This discrepancy along with others point to SN 2005hk and several other SNe Iax — and perhaps all SNe Iax — to have a wind component at late times. A two-component model consisting of the SN ejecta and a wind, either driven from a remnant or companion, solves the radius problem, the slow decline of the late-time light curve, the lack of velocity evolution of the photosphere from about 200 d to >400 d after peak brightness, and the fact that SNe Iax have a photosphere even at extremely late times.

For the two-component model, the photosphere, P-Cygni features, and narrow forbidden lines are caused by the wind while the broad forbidden lines are from the SN ejecta. In this case, the two components would be relatively decoupled. However, the details of the progenitor and explosion likely affect both the SN ejecta (through the amount of ^{56}Ni generated, the ejecta mass, the ejecta velocity, and the ejecta composition) and the wind (through the amount of ^{56}Ni trapped in the remnant, the mass of the remnant, and the composition of the remnant). Such a model may have compositional differences, which can be tested with detailed modeling.

We consider if SNe Iax are primarily asymmetric explosions. While not fully explored in current SN Iax models (Jordan et al. 2012; Kromer et al. 2013, 2015), it is possible that the explosion is highly asymmetric. However, the current spectroscopic data for a single SN Iax disfavour large asymmetries (Chornock et al. 2006; Maund et al. 2010). Although such extreme asymmetries currently seem unlikely, additional data will test if SN Iax explosions are generally symmetric.

We found that the low-luminosity SN 2008ha had a spectrum similar to the $\gtrsim 200$ d spectra of other SNe Iax only ~ 1 month after peak brightness. As SN 2008ha likely did not unbind its progenitor star (Foley et al. 2009, 2010b, 2013, 2014), it is an excellent candidate for having a bound remnant and wind. This early transition to a “wind-dominant” spectrum can possibly be explained by the relative amounts of ^{56}Ni in the remnant and ejecta (Kromer et al. 2015). Detailed spectral sequences, especially for low-luminosity events are necessary to determine if the timing of this transition is related to the explosion energetics.

Finally, we examined the spectra of SN 2014dt in detail, focusing on the possibility of there being dust and/or circumstellar material (as suggested by Fox et al. 2015). We find no evidence for newly formed or circumstellar dust, or any other circumstellar material, and the existing data disfavour dust emission as the source of the IR flux. As an alternative, the strong IR flux seen about 315 d after peak is perhaps caused by an extended optically thick super-Eddington wind. Such a scenario is consistent with all existing data. If

this emission is dominated by the remnant, it may be the second such detection after SN 2008ha (Foley et al. 2014).

Late-time spectra of future SNe Iax will continue to constrain their progenitors and explosions. Such data are critical for understanding the potential remnant star and the properties of a possible remnant-blown wind.

ACKNOWLEDGEMENTS

Facility: SOAR (Goodman), Keck:I (LRIS), Shane (Kast Double spectrograph), SALT (RSS)

R.J.F. gratefully acknowledges support from NSF grant AST-1518052 and the Alfred P. Sloan Foundation. SN Iax research at Rutgers University is supported by NASA/HST grants GO-12913 and GO-12973 to S.W.J. This work was supported by the NSF under grants PHY 11-25915 and AST 11-09174. A.V.F.’s research was funded by NSF grant AST-1211916, the TABASGO Foundation, and the Christopher R. Redlich Fund.

We thank the participants of the “Fast and Furious: Understanding Exotic Astrophysical Transients” workshop at the Aspen Center for Physics, which is supported in part by the NSF under grant PHY-1066293. Some of the work presented in this manuscript was initiated there during discussions with L. Bildsten & D. Kasen. Portions of this manuscript were also written during the Aspen Center for Physics workshop, “The Dynamic Universe: Understanding ExaScale Astronomical Synoptic Surveys.” We are grateful to the Aspen Center for Physics for its hospitality during the “Fast and Furious” and “Dynamic Universe” workshops in June 2014 and May 2015, respectively.

This research has made use of the NASA/IPAC Extragalactic Database (NED) which is operated by the Jet Propulsion Laboratory, California Institute of Technology, under contract with the National Aeronautics and Space Administration (NASA). Based in part on observations obtained at the Southern Astrophysical Research (SOAR) telescope, which is a joint project of the Ministério da Ciência, Tecnologia, e Inovação (MCTI) da República Federativa do Brasil, the U.S. National Optical Astronomy Observatory (NOAO), the University of North Carolina at Chapel Hill (UNC), and Michigan State University (MSU). KAIT and its ongoing operation were made possible by donations from Sun Microsystems, Inc., the Hewlett-Packard Company, AutoScope Corporation, Lick Observatory, the NSF, the University of California, the Sylvia & Jim Katzman Foundation, and the TABASGO Foundation. Research at Lick Observatory is partially supported by a generous gift from Google. Some of the data presented herein were obtained at the W. M. Keck Observatory, which is operated as a scientific partnership among the California Institute of Technology, the University of California, and NASA; the observatory was made possible by the generous financial support of the W. M. Keck Foundation. This research has made use of the Keck Observatory Archive (KOA), which is operated by the W. M. Keck Observatory and the NASA Exoplanet Science Institute (NExSci), under contract with NASA. We thank the staffs of the various observatories and telescopes (SOAR, Keck, SALT, Lick) where data were obtained, as well as observers who helped obtain some of the data (see Table A2).

APPENDIX A: REASSESSMENT OF PTF CLASSIFICATIONS

[White et al. \(2015\)](#) presented spectra and light curves of several SNe discovered by the (Intermediate) Palomar Transient Factory [(i)PTF]. The intent of their investigation was to construct a sample of SNe Iax and SNe similar to the low-velocity and peculiar Type I SN 2002es ([Ganeshalingam et al. 2012](#)).

To select their sample, [White et al. \(2015\)](#) examined SNe I in the (i)PTF sample. They then compared their spectra to those of previously classified SNe using `superfit` ([Howell et al. 2005](#)), allowing the redshift to vary by ± 0.02 . If one of the top 15 spectral matches was a SN Iax or SN 2002es, it was investigated further. After smoothing the spectrum, they measured the number of “peaks” seen in the spectrum between 6000 and 8000 Å. SNe with a large number of measured peaks were retained in the sample; however, the exact number necessary for inclusion in the final sample is not mentioned and some spectra do not cover this full spectral range. SNe that then have a strong Ti II $\lambda 4200$ line are considered SN 2002es-like (although one SN in their sample does not definitely have this feature), while those lacking this line and having a “peak” near 6200 Å are considered SNe Iax. In total, [White et al. \(2015\)](#) presented six new SNe classified as Type Iax and three new SNe classified as SN 2002es-like.

[White et al. \(2015\)](#) also re-evaluated literature SNe to determine if they were SNe Iax and/or SN 2002es. Their main conclusion from this additional investigation is that SNe 2004cs and 2007J, which have prominent He I lines in their spectra but are otherwise very similar to other SNe Iax ([Foley et al. 2009, 2013](#)), should be classified as SNe IIB instead of SNe Iax.

As part of our study of late-time spectra of SNe Iax, we examined the [White et al. \(2015\)](#) sample to determine if any members should be included in the current study. While only one SN in their sample (PTF09ego) has a spectrum at > 200 d after peak brightness, we examined the entire sample for completeness. Through this analysis, we found that four SNe are likely SNe Iax and two SNe are probably SN 2002es-like SNe. However, we show below that two SNe were misclassified and that one SN has insufficient data for a clear classification. Below we examine these misclassified and ambiguous SNe in detail.

Additionally, we re-evaluate the claim that SNe 2004cs and 2007J are SNe IIB. There is no strong evidence that SNe 2004cs and 2007J are SNe IIB, but significant evidence against this claim. In addition to other data, there is no evidence for hydrogen emission, arguing against the “Type II” designation. While it is still unclear if SNe 2004cs and 2007J are physically linked to SNe Iax (as discussed by [F13](#)), they do not appear to be SNe IIB.

A1 PTF09ego

PTF09ego was discovered with PTF imaging and reported by [White et al. \(2015\)](#); however, no discovery information is explicitly listed. Using two spectra, obtained on 23 September 2009 (at +13 d) and 15 May 2010 (at +225 d), [White et al. \(2015\)](#) classified PTF09ego as a SN Iax.

We retrieved these spectra from WISERep ([Yaron &](#)

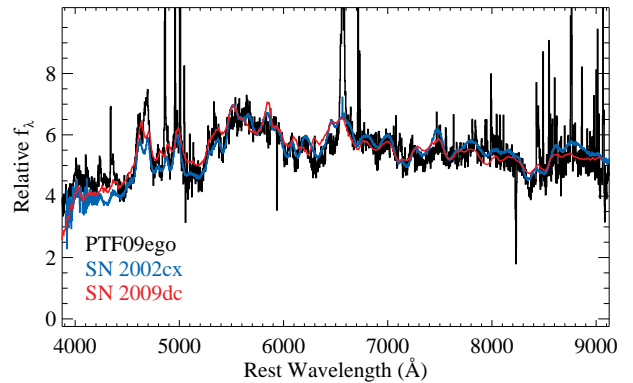


Figure A1. Optical spectrum of PTF09ego (black curve) as presented by [White et al. \(2015\)](#). Also shown are spectra of the SN Iax 2002cx (blue curve; [Li et al. 2003](#)) and the luminous SN Ia 2009dc (red curve; [Taubenberger et al. 2011](#)) at phases of +20 and +31 d, respectively. The spectra of SNe 2002cx and 2009dc have had a galaxy template spectrum added to roughly match the continuum seen in the spectrum of PTF09ego.

[Gal-Yam 2012](#)). The later spectrum, although noisy, is consistent with being primarily or all galaxy light. Therefore, it cannot be included in the current study. Furthermore, the early-time spectrum, while similar to that of SN 2002cx (see [Figure A1](#)), is equally similar to that of the high-luminosity SN Ia 2009dc (e.g., [Silverman et al. 2011; Taubenberger et al. 2011](#)), sometimes referred to as a “super-Chandrasekhar” SN Ia. While the peak luminosity of PTF09ego reported by [White et al. \(2015, \$M_R = -18.6\$ mag\) is more consistent with being a SN Iax, their reported rise time of \$\sim 21\$ d is significantly longer than that of any other SN Iax \(\$t_{\text{rise}} \approx 15\$ d\) and more consistent with SN 2009dc \(\$t_{\text{rise}} \approx 23\$ d; e.g., \[Silverman et al. 2011\]\(#\)\). Similarly, its relatively slow decline rate is similar to that of SN 2009dc and related objects.](#)

Although PTF09ego may be a SN Iax, an alternative explanation is that it is similar to SN 2009dc with significant host-galaxy dust reddening. We therefore consider PTF09ego to have an ambiguous classification. Regardless, its low-S/N late-time spectrum is not of adequate quality to be included in the current study.

A2 PTF09eiy

PTF09eiy was discovered with PTF imaging and reported by [White et al. \(2015\)](#); however, no discovery information is explicitly listed. They present five spectra of the SN with phases of roughly (the time of maximum brightness is not well measured) +14, +33, +63, +100, and +121 d. We present the three spectra having relatively high S/N in [Figure A2](#).

[White et al. \(2015\)](#) classify this SN as a SN Iax despite having high velocities (-9600 km s^{-1}) in their first spectrum. This spectrum differs from every other SN Iax spectrum in the [F13](#) and [White et al. \(2015\)](#) samples⁴. The

⁴ [White et al. \(2015\)](#) state that SN 2003gq, a SN Iax in the [F13](#) sample, has a velocity of about $-10,000 \text{ km s}^{-1}$ a week before maximum brightness. However, [F13](#) used this spectrum to mea-

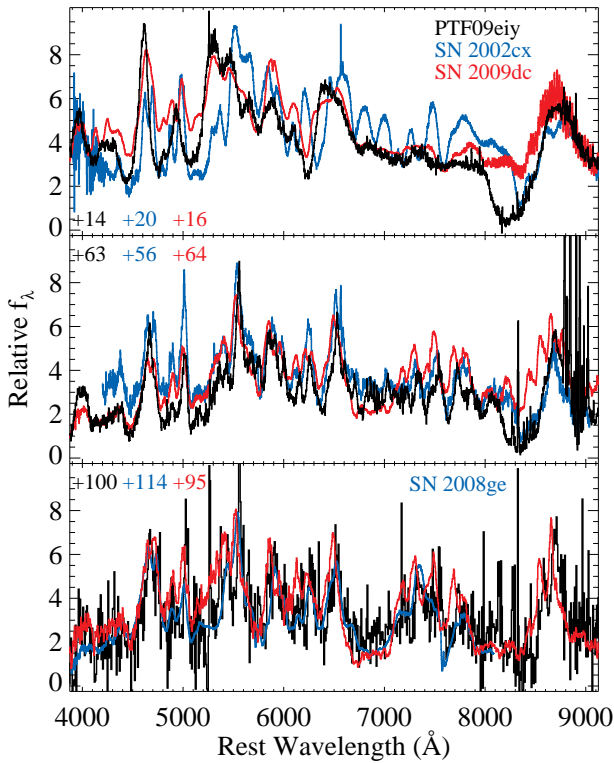


Figure A2. Optical spectra of PTF09eiy (black curve) as presented by White et al. (2015). Also shown are spectra of the SN Iax 2002cx (blue curve; Li et al. 2003), the SN Iax 2008ge (Foley et al. 2010a), and the luminous SN Ia 2009dc (red curve; Silverman et al. 2011; Taubenberger et al. 2011). The SN 2009dc spectra have been reddened by $E(B - V) = 0.45$ mag (corresponding to $A_V = 1.4$ mag).

classification appears to be mostly based on the later spectra, which are similar to spectra of SNe Iax at comparable phases (assuming that the SN was discovered near peak) and with the assumed redshift of 0.06.

Examining the PTF09eiy spectra in detail, we find that the later spectra are similar to those of other SNe Iax. However, the first spectrum is very different from any other SN Iax. This first spectrum is similar to those of typical SNe Ia at similar phases, but the later spectra are unlike any spectra of typical SNe Ia.

An alternative scenario is that PTF09eiy is not a SN Iax, but rather an atypical SN Ia similar to the high-luminosity SN Ia SN 2009dc (e.g., Silverman et al. 2011; Taubenberger et al. 2011). Figure A2 presents spectral comparisons between PTF09eiy and both SNe Iax and SN 2009dc at similar phases. For this comparison, SN 2009dc has been artificially extinguished by $A_V = 1.4$ mag, corresponding to a reddening of $E(B - V) = 0.45$ mag. After applying this reddening, SN 2009dc is similar to PTF09eiy at all phases.

According to White et al. (2015), PTF09eiy peaked at $M_R < -18.0$ mag. If we correct for an extinction of

sure a velocity of -5600 km s^{-1} , which we verified during the present analysis.

$A_V = 1.4$ mag, this corresponds to $M_R < -19.1$ mag; however, SN 2009dc may itself have $A_V \approx 0.9$ mag (Silverman et al. 2011), for which we did not correct in the spectral comparisons. Adopting this additional extinction, PTF09eiy peaked at $M_R < -20.0$ mag, significantly brighter than most SNe Ia.

Given the spectral similarity at all available epochs as well as consistent luminosities, we believe PTF09eiy is more likely to be similar to SN 2009dc than an atypical SN Iax.

A3 PTF10bvr

PTF10bvr was discovered with PTF imaging and reported by White et al. (2015); however, no discovery information is explicitly listed. Using a spectrum obtained 7.64 March 2010 (PI Kulkarni; Program C247LA) with the Low Resolution Imaging Spectrometer (LRIS; Oke et al. 1995), they classify PTF10bvr as a SN 2002es-like SN at $z = 0.015$. SN 2002es is a peculiar Type I SN similar to SN 1991bg in many regards, but having significantly lower ejecta velocity (Ganeshalingam et al. 2012). Because of their low expansion velocities, SNe 2002es-like objects may be physically related to SNe Iax.

While the nominal host galaxy of PTF10bvr, CGCG 224-067, is an early-type galaxy at $z = 0.02954$, White et al. (2015) claim to detect a strong Na D absorption line at $z = 0.015$ and use that redshift to classify the SN as having low velocities. There is no other possible host galaxy detected in any images presented by White et al. (2015), although presumably it would need to have a low luminosity in order to be closer than CGCG 224-067 yet remain undetected.

We obtained the LRIS data from the Keck Observatory Archive and rereduced the data using our own data-reduction pipeline. Standard CCD processing and spectrum extraction were accomplished with IRAF. The data were extracted using the optimal algorithm of Horne (1986). Low-order polynomial fits to calibration-lamp spectra were used to establish the wavelength scale, and small adjustments derived from night-sky lines in the object frames were applied. We employed our own IDL routines to flux calibrate the data and remove telluric lines using the well-exposed continua of spectrophotometric standards (Wade & Horne 1988; Foley et al. 2003; Silverman et al. 2012).

There were two standard-star observations obtained during the night: G191B2B and BD+33°2642. We used the former and latter to calibrate the blue and red data, respectively. However, BD+33 2642 is not an ideal standard as its absorption lines, particularly the Paschen series, make defining a continuum in regions of the spectrum affected by telluric absorption difficult. We carefully removed these features from our spectrum, but caution that the final result may still have residual problems.

Both our reduction and the White et al. (2015) reduction of the spectrum are presented in Figure A3. Examining the two, it is clear that the White et al. (2015) version suffers from several data-quality issues. First, the wavelength solution near the dichroic (covering at least $5500 - 6150 \text{ \AA}$) is incorrect by up to 40 \AA . Second, the flux beyond 9000 \AA is likely significantly underestimated; this was verified by independently reducing other spectra obtained during the night. The low flux at these wavelengths is perhaps partially

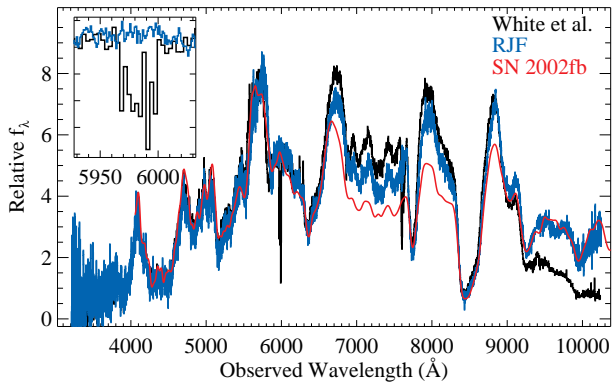


Figure A3. Optical spectrum of PTF10bvr. The black spectrum was reduced by M. Kasliwal and presented by [White et al. \(2015\)](#). The blue spectrum is a rereduction of the same data by one of us (R.J.F.). We note that the [White et al. \(2015\)](#) version appears to have been binned. The red spectrum is a smoothed spectrum of SN 2002fb, a SN 1991bg-like SN, at a phase of +18 d ([Silverman et al. 2012](#)), and shifted to be at the redshift of CGCG 224-067, $z = 0.02954$. The inset shows the region near the claimed $z = 0.015$ Na D absorption, which is only present in the previous reduction and is likely an artifact.

caused by a lack of telluric correction, which is evident as the telluric “A band” near 7600 Å is uncorrected.

We further examine the claimed Na D absorption. This feature is completely absent in the new reduction. Examining the two-dimensional image, there is a cosmic ray near the position of the object at roughly the correct wavelength, although this is in a region where the [White et al. \(2015\)](#) wavelength calibration is highly suspect, so it is difficult to confirm if that particular cosmic ray is causing the “absorption.” Close examination of the profile of this feature reveals that it does not have a typical shape and that its noise properties differ significantly from those of the continuum. We conclude that there is no Na D absorption, especially at $z = 0.015$, in the spectrum of PTF10bvr. A nearby cosmic ray on the detector is also a more likely scenario than PTF10bvr being hosted by a very low-luminosity galaxy in the direct foreground of a more luminous galaxy.

If we use the redshift of CGCG 224-067 as the redshift of PTF10bvr, it is clear that PTF10bvr is a SN 1991bg-like SN Ia, not similar to SN 2002es (Figure A3). Allowing the redshift to be a free parameter does not change the classification; the spectrum of PTF10bvr is much more similar to SN 1991bg-like objects at $z = 0.03$ than to SN 2002es at $z = 0.015$.

A4 SN 2004cs and SN 2007J

[Foley et al. \(2009\)](#) first noticed that SN 2007J was spectroscopically similar to other SNe Iax with the exception of strong He I lines present in the spectra of SN 2007J. [F13](#) identified SN 2004cs as a similar object, being spectroscopically similar to SNe Iax, but with strong He I lines. The possible physical association of these objects with the SN Iax class has far-reaching implications for the progenitors and explosions of SNe Iax, and was one of the strongest reasons

(but not the only one) that [F13](#) first suggested that SNe Iax had WD/He-star progenitor systems.

[White et al. \(2015\)](#) disagreed with this classification and claimed the detection of hydrogen lines in the spectra of both SNe, reclassifying these SNe as Type I Ib. We re-evaluate this claim here.

SN 2007J was relatively well observed with four spectra at distinct phases (see Figure A4). Although the exact time of maximum brightness was not measured, a nondetection was useful in constraining that time to within 40 d ([Foley et al. 2009, 2013](#)).

Examining these spectra, we do not detect any hydrogen lines in SN 2007J. Comparisons to SN 2002cx and SN I Ib 1996cb, the SN I Ib with the weakest H α emission at late times in the [Modjaz et al. \(2014\)](#) sample and the best-matching SN I Ib found, show that SN 2007J is more similar to SN 2002cx — even when considering the He I lines. This is especially true at early times, where there are significant deviations from SN 1996cb at bluer wavelengths. In particular, there is a strong H β line in the earliest spectrum of SN 1996cb, but no corresponding feature for SN 2007J. From this comparison alone, SN 2007J is highly discrepant with even the most similar SN I Ib known.

In addition to the lack of an H β line in SN 2007J, we note that the feature [White et al. \(2015\)](#) identified as H α in SN 2007J is also present in SN 2002cx and identified as Fe II by [Branch et al. \(2004\)](#). For SN 2007J, this feature is more similar to that of SN 2002cx at early times and evolves in a similar way (at later times the feature is relatively weak in all spectra). As SN 2002cx (and other SNe Iax) never show any strong hydrogen emission, including at late times, it is unlikely that this feature is H α in SN 2002cx, and similarly unlikely that it is H α in SN 2007J.

In conclusion, there is no evidence that SN 2007J is a SN I Ib. While SN 2007J may not be physically related to SNe Iax, it is most similar to these objects, and we consider this classification the most prudent at this time.

SN 2004cs does not have as much spectral data as SN 2007J; however, it does have a very constraining light curve presented by [F13](#). As presented by [F13](#) and re-examined here (Figure A5), SN 2004cs is very similar to SN 2007J as well as SN 2002cx (besides the He I lines). As was seen for SN 2007J, there are no obvious hydrogen lines in the spectrum of SN 2004cs. Based on the spectral data available, SN 2004cs is extremely similar to SN 2007J, and since SN 2007J is not a SN I Ib, it is unlikely that SN 2004cs is a SN I Ib.

There is stronger evidence against the SN I Ib classification for SN 2004cs based on its light curve (Figure A6), which is unlike that of any known SN I Ib. We reprocessed the unfiltered KAIT data presented by [F13](#) to improve the overall quality of the photometry and to include several nondetections before the SN rise and after it declined; see Table A1.

SN 2004cs rises to maximum light in <10 days and declines on a similar timescale. The new nondetections, including a relatively deep limit about 40 d after maximum, rule out a change in the decay rate right after the last detection. In contrast, the prototypical SN I Ib 1993J ([Richmond et al. 1994](#)), the well-observed SN I Ib 2011dh ([Arcavi et al. 2011; Ergon et al. 2014](#)), and the hydrogen-weak SN I Ib 1996cb ([Qiu et al. 1999](#)) all have much broader light curves and a

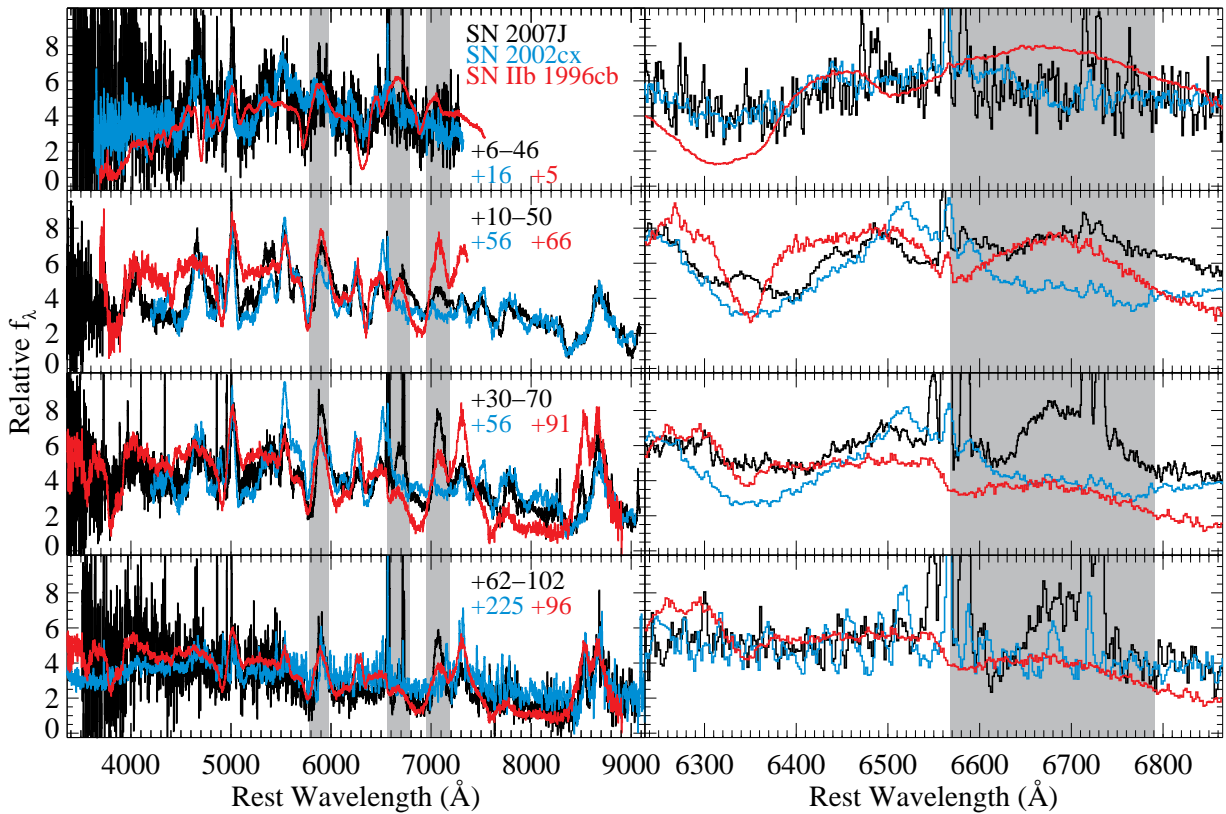


Figure A4. Optical spectra of SN 2007J (black curve). The phase ranges for the spectra are noted in each panel; the exact phase is not known, but is constrained by a nondetection and the first detection (see Foley et al. 2009, 2013). The left-side panels show the entire optical range, while the right-side panels display in detail the area around $H\alpha$. There is no broad $H\alpha$ from SN 2007J visible in any spectrum. Comparison spectra of SN Iax 2002cx and SN Iib 1996cb are shown as blue and red curves, respectively, with phases also noted. SN 1996cb was specifically chosen as the SN Iib with the weakest $H\alpha$ emission at late times (to match the lack of obvious $H\alpha$ in SN 2007J). Regions corresponding to the strong $He\text{I } \lambda\lambda 5876, 6678, 7065$ lines are shaded grey.

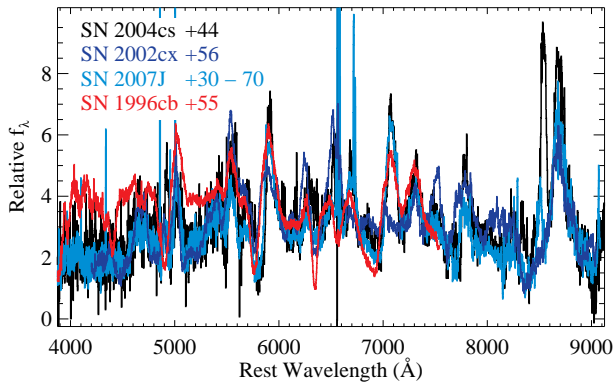


Figure A5. Optical spectrum of SN 2004cs (black curve); there is no obvious broad $H\alpha$ in the spectrum. Similar-phase comparison spectra of SN Iax 2002cx, SN 2007J, and SN Iib 1996cb are shown as dark blue, light blue, and red curves, respectively.

change in decay rate occurring between 20 d and 40 d after peak. White et al. (2015) found that the light curve of SN 2004cs was consistent with the SN Iib template light curve of Arcavi et al. (2012); however, this comparison indicated that SN 2004cs declined faster than the template. In

addition, the comparison presented by White et al. (2015) is not ideal. They used the start of the template light curve as the time of maximum, but the Arcavi et al. (2012) template begins roughly 5 d after maximum, when the light curve is declining much faster than right at peak. The template also only covers ~ 12 days of the light curve, and so the comparison ignores all premaximum data and the later data where SN 2004cs continues to quickly decline while SNe Iib decline slower at these phases. Finally, this template was generated from only two light curves, with one having only 5 data points over 36 days (and 3 at maximum brightness or later), so this template is not the best comparison when excellent data, such as those for SNe 1993J and 2011dh, exist.

In addition, SN 2004cs does not have the initial peak and decline before rising to maximum that is associated with the cooling of a shocked stellar envelope and is seen in many SNe Iib, including SNe 1993J and 2011dh. While this has not been detected in all SNe Iib (e.g., SN 1996cb; Figure A6), it has for those SNe with deep, high-cadence observations around the time of explosion, like what was obtained for SN 2004cs. Therefore, the deep nondetections before the rise are highly constraining and indicate that SN 2004cs was not a SN Iib. Furthermore, it is unclear if a SN Iib progenitor could produce such a rapidly evolving light curve (requiring very small ejecta mass).

Table A1. KAIT Unfiltered Light Curve of SN 2004cs

| MJD | Mag | σ (mag) | Limit (mag) |
|-----------|-------|----------------|-------------|
| 53164.412 | ... | ... | 19.7 |
| 53165.426 | ... | ... | 19.8 |
| 53166.423 | ... | ... | 19.3 |
| 53168.436 | ... | ... | 19.1 |
| 53169.412 | ... | ... | 19.7 |
| 53173.431 | ... | ... | 19.7 |
| 53175.397 | ... | ... | 20.0 |
| 53177.399 | 19.35 | 0.18 | ... |
| 53179.405 | 18.15 | 0.06 | ... |
| 53180.203 | 17.95 | 0.06 | ... |
| 53180.388 | 17.91 | 0.06 | ... |
| 53182.394 | 17.66 | 0.06 | ... |
| 53184.353 | 17.51 | 0.06 | ... |
| 53187.371 | 17.57 | 0.08 | ... |
| 53193.387 | 18.07 | 0.07 | ... |
| 53195.312 | 18.20 | 0.09 | ... |
| 53197.323 | 18.40 | 0.08 | ... |
| 53199.318 | 18.67 | 0.10 | ... |
| 53200.287 | 18.82 | 0.14 | ... |
| 53204.359 | 18.97 | 0.16 | ... |
| 53206.296 | 19.12 | 0.12 | ... |
| 53208.270 | ... | ... | 19.3 |
| 53210.259 | ... | ... | 19.3 |
| 53212.241 | ... | ... | 19.4 |
| 53214.261 | ... | ... | 19.0 |
| 53216.231 | ... | ... | 18.7 |
| 53218.242 | ... | ... | 19.2 |
| 53219.296 | ... | ... | 19.2 |
| 53221.272 | ... | ... | 19.4 |
| 53222.272 | ... | ... | 19.5 |
| 53226.230 | ... | ... | 20.0 |

Finally, [Rajala et al. \(2005\)](#) measured a single epoch of multiband photometry for SN 2004cs at ~ 5 d before maximum brightness, finding colours that were significantly inconsistent with those of SNe I Ib as well as all core-collapse SNe. However, the colours were consistent with those of a young SN Ia, whose colours are similar to those of SNe Iax.

In summary, SN 2004cs has a spectrum similar to that of SN 2007J as well as SN 2002cx (besides the prominent He I lines). While SN 2004cs is spectroscopically similar to some SNe I Ib (although we cannot confirm any hydrogen in its spectrum), its light curve is unlike that of any SN I Ib, rising faster and declining faster than any known SN I Ib. Furthermore, SN 2004cs lacks the signature of a cooling envelope seen in all SNe I Ib with similar-quality data. From this, we conclude that it is highly unlikely that SN 2004cs is a SN I Ib, while being very similar to SNe Iax.

A5 Summary and Discussion

Above, we showed that PTF09ego may not be a SN Iax, that PTF09ey is unlikely to be a SN Iax and more likely to be similar to SN 2009dc and other high-luminosity SNe Ia, and that PTF10bvr is not a SN 2002es-like SN. None the less, 6/9 of the [White et al. \(2015\)](#) sample appear to be likely SNe Iax or SN 2002es-like objects.

We also re-examine the claims of [Foley et al. \(2009\)](#) and [F13](#) that SNe 2004cs and 2007J are SNe Iax and not SNe I Ib

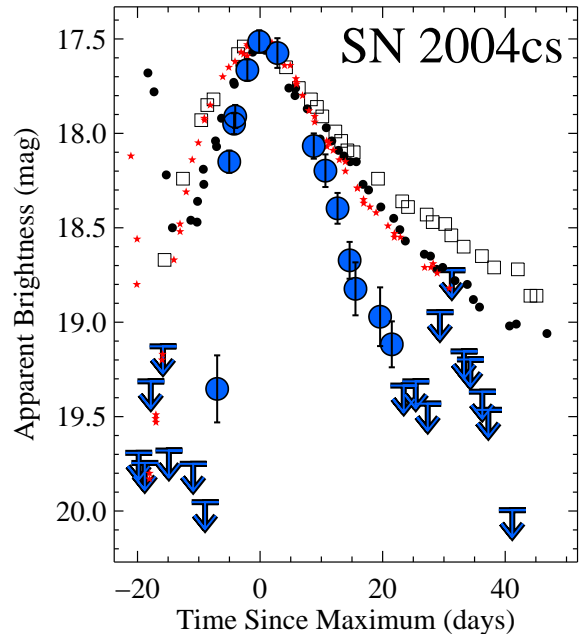


Figure A6. Unfiltered KAIT light curve of SN 2004cs (blue circles, and blue arrows indicating upper-limit nondetections). Also displayed are *R*-band (similar to unfiltered) light curves of SNe 1993J (black circles; [Richmond et al. 1994](#)), 1996cb (squares; [Qiu et al. 1999](#)), and 2011dh (red stars; [Arcavi et al. 2011](#); [Ergon et al. 2014](#)), all shifted to match the peak of SN 2004cs.

as claimed by [White et al. \(2015\)](#). We find no evidence of these SNe being SNe I Ib and strong evidence against this classification. We also show that other than the presence of He I lines, they are very similar to SNe Iax. We therefore continue to classify SNe 2004cs and 2007J as SNe Iax, although we also caution that observations of similar SNe in the future may indicate that SNe 2004cs and 2007J are physically distinct from SNe Iax.

One of the main goals of [White et al. \(2015\)](#) was to measure the relative rate of SNe Iax and SNe Ia, finding 5.6 SNe Iax (and SN 2002es-like objects) per 100 SNe Ia. This value was much smaller than that found by [F13](#), 31 SNe Iax per 100 SNe Ia (and not counting SN 2002es-like objects). While the reclassification of up to 1/3 of the [White et al. \(2015\)](#) sample may point to an even lower rate, we caution against this conclusion.

We first note that [White et al. \(2015\)](#) did not correct for the photometric and spectroscopic selection of their survey. Considering that SNe Iax are 1–5 mag fainter than typical SNe Ia at peak and typically fade twice as fast as SNe Ia, there must be some photometric selection bias. Additionally, the contrast of relatively faint SNe Iax compared to their host galaxies likely makes detecting the SNe more difficult, and may (partially) explain the large fraction of relatively low-surface brightness host galaxies in their sample.

Similarly, the [White et al. \(2015\)](#) sample almost certainly suffers from spectroscopic selection bias. They mention nine SNe that have some spectroscopic similarities to SNe Iax and SN 2002es, but most were rejected from the final sample because of low-S/N spectra. These additional objects alone could double the measured rate.

We further note that of the six White et al. (2015) SN Iax candidates, the earliest spectra were obtained at +13, +14, +23, +25, +26, and +56 d relative to maximum brightness, with the earliest spectra coming from PTF09ego (which is perhaps not a SN Iax) and PTF09eiy (which is unlikely to be a SN Iax). However, 30–55% of the PTF SN Ia sample have at least one spectrum before +5 d (Maguire et al. 2014). Assuming that the PTF SN Ia and SN Iax spectroscopic selection functions are identical and adopting the most favourable conditions, there is only a 12% chance of having no SN Iax in the White et al. (2015) sample with a spectrum before +5 d (0.8% assuming the higher fraction (55%) with early-time spectra, and it is further unlikely to have no spectra between +5 and +13 d and extremely unlikely to have no spectra before +23 d, which is the earliest spectrum of a definitive SN Iax in the sample). Considering that SNe Iax are less luminous than SNe Ia, one would expect relatively *more* spectra near maximum light for this class.

One likely reason for this discrepancy is the method for selecting members of the class. White et al. (2015) make two decisions that probably bias against selecting SNe Iax near maximum brightness. The first is that they only selected SNe where `superfit` returned a match with a SN Iax in its top 15 matches. However, it is well known (e.g., Li et al. 2003; J06) that near maximum brightness, SN Iax spectra are very similar to those of SNe Ia except for their velocity, which is degenerate with redshift when doing a χ^2 fit as `superfit` does. In fact, 12 of the 25 SNe Iax in the F13 sample were at some point misclassified, often because of this effect.

To test this possibility, we classified the -1 d spectrum of SN 2002cx (Li et al. 2003) using SNID (Blondin & Tonry 2007). Although SNID is a different algorithm than `superfit`, this experiment is illustrative. With no prior on the redshift, there were no SNe Iax in the top 20 spectral matches. Putting the correct prior on the redshift, the SN is still not correctly classified, with no SNe Iax in the top 15 spectral matches. Therefore, SNe without host-galaxy redshifts are particularly prone to misclassification. This problem is likely amplified with noisy data.

An additional selection bias is the “peak counting” employed by White et al. (2015). Starting ~ 2 weeks after maximum light, SNe Iax have very complex spectra with many distinct spectral features. However, this is not the case near maximum brightness. While White et al. (2015) do not explicitly state how many peaks (in the range 6000 – 8000 Å) are necessary for inclusion in their final sample, it appears to be around 7 given the objects that were included. Although there is no description of exactly how significant a peak must be to be counted, we attempted this analysis for SN Iax 2011ay, which has one of the best spectral sequences between peak and +30 d (F13). We find that the spectra spanning phases of -2 to $+11$ d all have < 7 peaks, while the spectra after $+26$ d all have ≥ 7 peaks. Therefore, if there were only a single maximum-light spectrum of SN 2011ay, it would likely be excluded from the White et al. (2015) analysis, even if it passes the `superfit` criterion.

While the smaller sample of genuine SNe Iax in the White et al. (2015) sample may, at first glance, appear to make the relative rate even less consistent with the rate of F13, the various photometric biases, spectroscopic biases,

sample-selection biases, and already identified ambiguous objects are likely the reasons for the difference.

As further confirmation of the “high” rate of F13, we recalculate the relative rate using only SNe within $D \lesssim 20$ Mpc. In the last 10 yr, there have been 5 SNe Iax discovered within this volume: SNe 2008ge (Foley et al. 2010a), 2008ha (Foley et al. 2009, 2010b; Valente et al. 2009), 2010ae (Stritzinger et al. 2014), 2010el, and 2014dt (Foley et al. 2015). During this same time, there were ~ 25 SNe Ia discovered in this volume. Without any additional corrections, this places a very robust lower limit on the relative rate of ~ 24 SNe Iax for every 100 SNe Ia, consistent with the F13 rate and significantly inconsistent with the White et al. (2015) rate.

REFERENCES

- Arcavi I., et al., 2011, *ApJ*, **742**, L18
 Arcavi I., et al., 2012, *ApJ*, **756**, L30
 Blondin S., Tonry J. L., 2007, *ApJ*, **666**, 1024
 Bose S., Kumar B., 2014, *ApJ*, **782**, 98
 Branch D., Baron E., Thomas R. C., Kasen D., Li W., Filippenko A. V., 2004, *PASP*, **116**, 903
 Chornock R., Filippenko A. V., Branch D., Foley R. J., Jha S., Li W., 2006, *PASP*, **118**, 722
 Clemens J. C., Crain J. A., Anderson R., 2004, in Moorwood A. F. M., Iye M., eds, Society of Photo-Optical Instrumentation Engineers (SPIE) Conference Series Vol. 5492, Ground-based Instrumentation for Astronomy. pp 331–340, doi:10.1117/12.550069
 Crawford S. M., et al., 2010, in Society of Photo-Optical Instrumentation Engineers (SPIE) Conference Series. p. 773725, doi:10.1117/12.857000
 Ergon M., et al., 2014, *A&A*, **562**, A17
 Filippenko A. V., 2003, in Hillebrandt W., Leibundgut B., eds, From Twilight to Highlight: The Physics of Supernovae. p. 171 (arXiv:astro-ph/0307138), doi:10.1007/10828549_23
 Foley R. J., 2013, *MNRAS*, **435**, 273
 Foley R. J., et al., 2003, *PASP*, **115**, 1220
 Foley R. J., et al., 2009, *AJ*, **138**, 376
 Foley R. J., et al., 2010a, *AJ*, **140**, 1321
 Foley R. J., Brown P. J., Rest A., Challis P. J., Kirshner R. P., Wood-Vasey W. M., 2010b, *ApJ*, **708**, L61
 Foley R. J., et al., 2013, *ApJ*, **767**, 57
 Foley R. J., McCully C., Jha S. W., Bildsten L., Fong W.-f., Narayan G., Rest A., Stritzinger M. D., 2014, *ApJ*, **792**, 29
 Foley R. J., Van Dyk S. D., Jha S. W., Clubb K. I., Filippenko A. V., Mauerhan J. C., Miller A. A., Smith N., 2015, *ApJ*, **798**, L37
 Fox O. D., et al., 2015, preprint, (arXiv:1510.08070)
 Ganeshalingam M., et al., 2012, *ApJ*, **751**, 142
 Hatano K., Branch D., Fisher A., Millard J., Baron E., 1999, *ApJS*, **121**, 233
 Horne K., 1986, *PASP*, **98**, 609
 Howell D. A., et al., 2005, *ApJ*, **634**, 1190
 Jha S., Branch D., Chornock R., Foley R. J., Li W., Swift B. J., Casebeer D., Filippenko A. V., 2006, *AJ*, **132**, 189
 Jordan IV G. C., Perets H. B., Fisher R. T., van Rossum D. R., 2012, *ApJ*, **761**, L23
 Kelly B. C., 2007, *ApJ*, **665**, 1489
 Kelly P. L., et al., 2014, *ApJ*, **790**, 3
 Kromer M., et al., 2013, *MNRAS*, **429**, 2287
 Kromer M., et al., 2015, *MNRAS*, **450**, 3045
 Li W., et al., 2003, *PASP*, **115**, 453
 Li W., et al., 2011, *Nature*, **480**, 348

- Liu Z.-W., Stancliffe R. J., Abate C., Wang B., 2015, preprint, ([arXiv:1506.04903](https://arxiv.org/abs/1506.04903))
- Maguire K., et al., 2014, *MNRAS*, **444**, 3258
- Maund J. R., et al., 2010, *ApJ*, **722**, 1162
- McCully C., et al., 2014a, *Nature*, **512**, 54
- McCully C., et al., 2014b, *ApJ*, **786**, 134
- Miller J. S., Stone R. P. S., 1993, Lick Obs. Tech. Rep. 66. Santa Cruz: Lick Obs.
- Modjaz M., et al., 2014, *AJ*, **147**, 99
- Nakano S., Itagaki K., 2014, CBET, 4011
- Narayan G., et al., 2011, *ApJ*, **731**, L11+
- Ochner P., Tomasella L., Benetti S., Cappellaro E., Elias-Rosa N., Pastorello A., Turatto M., 2014, The Astronomer's Telegram, **6648**, 1
- Oke J. B., et al., 1995, *PASP*, **107**, 375
- Phillips M. M., et al., 2007, *PASP*, **119**, 360
- Qiu Y., Li W., Qiao Q., Hu J., 1999, *AJ*, **117**, 736
- Rajala A. M., et al., 2005, *PASP*, **117**, 132
- Richmond M. W., Treffers R. R., Filippenko A. V., Paik Y., Leibundgut B., Schulman E., Cox C. V., 1994, *AJ*, **107**, 1022
- Rodríguez Ó., Clocchiatti A., Hamuy M., 2014, *AJ*, **148**, 107
- Sahu D. K., et al., 2008, *ApJ*, **680**, 580
- Schoeniger F., Sofue Y., 1997, *A&A*, **323**, 14
- Silverman J. M., Ganeshalingam M., Li W., Filippenko A. V., Miller A. A., Poznanski D., 2011, *MNRAS*, **410**, 585
- Silverman J. M., et al., 2012, *MNRAS*, **425**, 1789
- Smith M. P., Nordsieck K. H., Burgh E. B., Percival J. W., Williams T. B., O'Donohue D., O'Connor J., Schier J. A., 2006, in Society of Photo-Optical Instrumentation Engineers (SPIE) Conference Series. p. 62692A, [doi:10.1117/12.672415](https://doi.org/10.1117/12.672415)
- Smith N., Foley R. J., Filippenko A. V., 2008, *ApJ*, **680**, 568
- Stritzinger M. D., et al., 2014, *A&A*, **561**, A146
- Stritzinger M. D., et al., 2015, *A&A*, **573**, A2
- Taubenberger S., et al., 2011, *MNRAS*, **412**, 2735
- Thielemann F.-K., Nomoto K., Yokoi K., 1986, *A&A*, **158**, 17
- Timmes F. X., Brown E. F., Truran J. W., 2003, *ApJ*, **590**, L83
- Valenti S., et al., 2009, *Nature*, **459**, 674
- Wade R. A., Horne K., 1988, *ApJ*, **324**, 411
- White C. J., et al., 2015, *ApJ*, **799**, 52
- Yaron O., Gal-Yam A., 2012, *PASP*, **124**, 668

Table A2. Log of Spectral Observations of SN 2014dt

| Phase ^a | UT Date | Telescope / Instrument | Exposure (s) | Observer ^b |
|--------------------|------------------|---------------------------|-----------------|-----------------------|
| +172 | 2015 Apr. 16.406 | Lick/Kast | 1800 | IS |
| +204 | 2015 May 17.829 | SALT/RSS | 4 × 425 | AK |
| +212 | 2015 May 26.285 | Lick/Kast | 1800 | MG |
| +228 | 2015 June 11.718 | SALT/RSS | 4 × 425 | AK |
| +233 | 2015 June 16.068 | SOAR/Goodman | 2 × 1800 | RF, SD, YP |
| +233 | 2015 June 16.328 | Keck/LRIS | 600 | AF, MG, WZ |
| +270 | 2015 July 24.039 | SOAR/Goodman | 2 × 1800 | RF, RH, SD |
| +410 | 2015 Dec. 11.641 | Keck/LRIS | 2 × 1200 | MG, SV |

^aDays since *B* maximum, 2015 Oct. 25.2 (JD 2,456,955.7).

^bAF = A. Filippenko, IS = I. Shivvers, MG = M. Graham, AK = A. Kniazev, RF = R. Foley, RH = R. Hounsell, SD = S. Downing, SV = S. Valenti, WZ = W. Zheng, YP = Y.-C. Pan

Table A3. Forbidden-Line Fit Parameters

| SN | Phase (days) | Narrow Component | | | | | | | | | | Broad Component | | | | | |
|--------|-----------------|------------------------|------------------------|-------------------------------------|------------------------|------------------------|------------------------|--------------------------------|---------------------------------|------------------------|------------------------|------------------------|------------------------|---------------|------------|--|--|
| | | [Fe II] $\lambda 7155$ | | [Ca II] $\lambda\lambda 7291, 7324$ | | [Ni II] $\lambda 7378$ | | FWHM (km s^{-1}) | Shift (km s^{-1}) | [Fe II] $\lambda 7155$ | | [Ni II] $\lambda 7378$ | | | | | |
| | | Rel. Line Strength | EW (\AA) | Rel. Line Strength | EW (\AA) | Rel. Line Strength | EW (\AA) | | | Rel. Line Strength | EW (\AA) | Rel. Line Strength | EW (\AA) | | | | |
| 2002cx | +227 | 1430 (110) | 31 (41) | 1 | 37 (7) | 1.13 (0.21) | 83 (15) | 0.11 (0.10) | 3.9 (3.5) | 7870 (910) | 1130 (430) | 0.34 (0.10) | 69 (23) | 0.46 (0.10) | 90 (20) | | |
| 2005P | >+109 | 1570 (60) | 530 (27) | 1 | 77 (10) | 1.87 (0.24) | 288 (28) | 0.78 (0.12) | 59.9 (7.8) | 7950 (180) | 840 (110) | 0.95 (0.11) | 373 (28) | 1.27 (0.14) | 500 (30) | | |
| 2005hk | +224 | 680 (30) | -295 (13) | 1 | 62 (9) | 2.22 (0.26) | 273 (34) | 0.41 (0.09) | 25.2 (5.7) | 7050 (470) | -40 (260) | 0.14 (0.03) | 90 (19) | 0.35 (0.05) | 230 (40) | | |
| 2008A | +220 | 1490 (60) | 488 (27) | 1 | 126 (15) | 1.65 (0.19) | 416 (49) | 0.40 (0.10) | 50.0 (12.3) | 8440 (90) | -730 (40) | 0.83 (0.06) | 593 (28) | 2.64 (0.19) | 1880 (90) | | |
| 2008ge | +225 | 2680 (100) | 898 (38) | 1 | 151 (13) | ... | ... | 0.78 (0.10) | 117.5 (15.8) | 7080 (70) | 70 (20) | 0.83 (0.06) | 331 (16) | 2.84 (0.16) | 1140 (40) | | |
| 2010ae | +252 | 770 (50) | 54 (25) | 1 | 25 (5) | 6.93 (1.37) | 351 (62) | 0.16 (0.11) | 4.1 (2.7) | ... | ... | ... | ... | ... | ... | | |
| 2011ay | +176 | 3320 (270) | -1144 (72) | 1 | 18 (10) | 3.26 (1.95) | 116 (29) | 0.51 (0.97) | 9.1 (14.2) | 7700 (160) | -520 (110) | 7.43 (3.83) | 308 (32) | 21.55 (10.34) | 900 (60) | | |
| 2011ce | +371 | 780 (60) | 87 (26) | 1 | 12 (3) | 2.12 (0.43) | 51 (8) | 0.32 (0.13) | 3.8 (1.4) | ... | ... | ... | ... | ... | ... | | |
| 2012Z | +248 | 1790 (120) | -107 (45) | 1 | 115 (20) | 0.36 (0.10) | 84 (29) | 0.11 (0.12) | 12.6 (14.8) | 9000 (70) | -1380 (30) | 1.33 (0.11) | 773 (63) | 7.74 (0.52) | 4510 (310) | | |
| 2014dt | +233 | 950 (60) | -333 (25) | 1 | 30 (5) | 1.18 (0.20) | 72 (12) | 0.59 (0.14) | 17.9 (4.2) | 6400 (320) | 530 (160) | 0.32 (0.07) | 65 (11) | 0.95 (0.12) | 200 (20) | | |